Hydrology, Fluid Flux, and Chemical Travel Times through the Vadose Zone at Ehmke Playa in the Central High Plains of Kansas

By

Kaitlin A. Salley
B.Sc., Eastern Washington University, 2010

Submitted to the graduate degree program in Geology and the Graduate Faculty of the University of Kansas in partial fulfillment of the requirements for the degree of Master of Science.

_____

Chair: Randy L. Stotler

_____

William C. Johnson

_____

Leigh A. Stearns

Date Defended: 8 May 2018

The thesis committee for Kaitlin A. Salley certifies that this is the approved version of the following thesis:

Hydrology, Fluid Flux, and Chemical Travel Times through the Vadose Zone at Ehmke Playa in the Central High Plains of Kansas

Chair: Randy L. Stotler

Date Approved: 8 May 2018

Abstract

Groundwater levels of the High Plains aquifer (HPA) are declining in western Kansas, due mainly to large-scale irrigation pumping since the 1950s. Previous recharge rate estimates in the Central High Plains vary between 5 to 54 mm yr^{-1}, indicating infiltration to the water table takes at least 270 yrs through the 15 to 100 m-thick vadose zone. Despite this, aquifer contaminants related to agricultural practices since the 1950s suggest the existence of preferential flow and recharge pathways to the aquifer.

Playas, ephemeral lakes with hydric soil floors, are ubiquitous features (>22,000) across the High Plains in western Kansas, but are in decline due to anthropogenic modification. It is hypothesized that preferential recharge pathways to the HPA form in playa basins, primarily through desiccation cracks that develop in the hydric soil floors, which could facilitate rapid movement of water at the onset of rain events. This study aims to determine recharge rates at Ehmke Playa site in western Kansas and determine if this playa acts as significant point of recharge to the HPA.

Anion concentrations in the vadose zone are plotted against depth to visualize peaks and troughs, and better understand vertical flow. Vadose zone chloride concentrations are significantly higher beneath the interplaya (30 to 3,900 mg L^{-1}) than the playa (12 to 140 mg L^{-1}), which indicates slower chemical and water movement through the interplaya. Bromide, nitrate, sulfate, and fluoride depth profiles also show higher concentration beneath the interplaya. Some anion concentrations (chloride, bromide, and sulfate) exhibit a maxima at the base of the root zone (2 m), implying greater evapotranspiritive enrichment in the interplaya and lower fluid recharge flux than within the playa.

Utilizing the chloride mass balance (CMB) method, a fluid flux and travel time through the vadose zone is calculated using a ratio of chloride concentration input at the surface with chloride concentration in the vadose zone pore water. Fluid flux rates range between from 78 to 118 mm yr^{-1} for playa dry periods, 1,700 mm yr^{-1} during playa wet periods, and from 0.1 to 10 mm yr^{-1} for the interplaya. Travel times through the 11.5 m playa vadose zone (8 to 150 yrs) were at least an order of magnitude faster than through the 16.7 m interplaya vadose zone (4,800 to 5,500 yrs).

Matric potential (MP) sensors installed at four near-surface depths beneath the playa bottom indicate gravity drainage during playa ponding events. The uppermost sensor (12 cm below ground surface, bgs) exceeded field capacity (-33 kPa) on March 29 at 11:30 AM, likely from a rain event beginning March 23 at 8:00 PM and totaling 56.9 mm. Deeper MP intervals (47, 92, and 152 cm bgs) increased above field capacity much later (April 12 at 10:30 PM, April 13 at 9:20 AM, and April 14 at 3:20 AM, respectively) after a large precipitation event (79.3 mm) occurred on April 12 causing the playa to become inundated on April 13. This indicates deeper wetting is heavily dependent upon precipitation events resulting in playa inundation. Evidence of macropores was observed during inundation, when MP is higher at 96 cm than 47 cm, resulting in a zero flux plane (ZFP) around the 96 cm depth.

Soil saturated hydraulic conductivity (K_{sat}) was determined using an automated infiltrometer. Measurements in both the playa and interplaya range from 1.62 $x10^{-4}$ to 7.84 $x10^{-4}$ cm sec^{-1}, indicative of a silt loam soil. This value is representative of the playa during inundation, or of the interplaya when saturated during rain events.

Hourly water level measurements from pressure transducers in three monitoring wells at the site indicate groundwater flow is towards north 66° east and under a hydraulic gradient of

0.0016. Groundwater anion concentrations show the chloride/bromide mass ratio upgradient (0.004) is lower than downgradient (0.01), which indicates greater meteoric water influence on downgradient waters when compared to upgradient waters, again indicating recharge flux through the playa basin.

Combined, the data provide an overview of all hydrologic interactions at the Ehmke Playa site and constrains recharge rates. This study advances understanding of playa hydrology in the CHP by improving recharge estimates, analyzing preferential flow paths, and identifying the role of playas in the long-term sustainability and quality of the HPA. Further, data from this study can be used for more realistic water resource estimates, support of playa conservation, and improved management of the HPA.

Table of Contents

List of Tables

List of Figures

Supplementary Tables Appendix 1

Supplementary Figures Appendix 2

Introduction

The High Plains aquifer (HPA) extends across eight states, encompasses 450,656 km^2 (174,000 mi^2), and is responsible for approximately 23% of the total groundwater use nationally (Figure 1) (Gutentag et al., 1984; Maupin and Barber, 2005). In Kansas, approximately 3.36 billion m^3 (887 billion gallons, 2.72 million acre-ft,) was withdrawn in 2016, 91% of which was used for irrigation (Maupin and Barber, 2005; Water Information Management and Analysis System, 2018). Central Kansas annual recharge rates to the HPA are estimated around 925 million m^3 (244 billion gallons, 0.75 million acre-ft,), which is approximately 28% of the quantity pumped annually (Buchanan et al., 2015). This results in substantial reductions in the saturated aquifer thickness (Buchanan et al., 2015). In Kansas, large-scale groundwater development began in the 1950s, with the invention of the center-pivot irrigation system and improvements in drilling and pumping technology which resulted in less-expensive, more efficient wells (Gutentag et al., 1984; Buchanan et al., 2015). From predevelopment (1950) to 2014-2016, some areas of the aquifer have experienced over 60% reduction in the saturated thickness, with water levels declining by over 50 m (164 ft) in southwestern Kansas (McGuire, 2009; Scanlon et al., 2012; Buchanan et al., 2015). Although isolated regions in the northwest and central part of Kansas have witnessed water level increases since predevelopment, the majority of the Kansas HPA is experiencing water level declines (Scanlon et al., 2012; Buchanan et al., 2015). Under current pumping rates and average climatic conditions, water-level declines and water quality degradation will continue, likely compromising future use of the aquifer (Whittemore et al., 2016).

Recharge rates have been studied across the HPA and are spatially variable, with precipitation and recharge generally greater in the northern High Plains (NHP),

evapotranspiration generally greater in the southern High Plains (SHP), and the Central High Plains (CHP) between these two extremes (Figure 1) (Gurdak et al., 2007). Previously published recharge estimates for Kansas (5 to 54 mm yr^{-1}) indicate a travel time of 270 to over 1000 years for infiltrated water to travel through the 15 to 100 m-thick vadose zone to the aquifer (Gurdak et al., 2007). Notwithstanding, the presence of agricultural contaminants in the aquifer indicates recharge of modern water (since the 1950s), which is indicative of a <100-year travel time to the water table (McMahon et al., 2006). The faster paths to the aquifer are likely through focused recharge and preferential flow paths, including areas with ponded surface water such as ephemeral streambeds, ditches, shallow depressions, irrigated cropland and playas (Gurdak et al., 2007, 2008; Meixner et al., 2016). Fluid flux through these areas of preferential flow often exceeds diffuse recharge (>100 yrs), which represents movement of water between individual pore spaces. Preferential flow paths (e.g., macropores) are of particular interest in playas because they can move water very quickly (<100 yrs). This type of recharge bypasses some or all of the soil matrix through secondary porosity, utilizing natural features including desiccation cracks, root tubes, and animal and insect burrows (Gurdak and Roe, 2009).

Studies of recharge through the dense system of SHP playas has have concluded that measured playa recharge rates (60 to 120 mm yr^{-1}) are higher than diffuse recharge estimates (0.2 to 32 mm yr^{-1}) (Scanlon and Goldsmith, 1997; Wood et al., 1997; Gurdak et al., 2007; Johnson et al., 2012; Meixner et al., 2016). Additionally, it is estimated that macropore recharge, including through playas, accounts for a large percentage (84%) of the total average regional recharge in the SHP (11 mm yr^{-1}) (Wood et al., 1997).

Although playas are also abundant (>22,000) in Kansas (Figure 2), the possibility for recharge through Kansas playas to the HPA has not been investigated (Bowen, 2011). This is addressed in this research by determining water fluxes through a Kansas playa and interplaya, identifying time periods of downward fluid flux during playa inundation, and quantifying travel times to the HPA. Water flux and travel times through the vadose zone are determined using the Chloride Mass Balance (CMB), with additional information on fluid flow obtained from vadose zone anion depth profiles and matric potential (MP), groundwater chemistry, and water level changes.

Background

Playas are internally-drained (closed basin) ephemeral lakes with varying periods of inundation. The amount of time an individual playa remains inundated is known as the hydroperiod (Gurdak and Roe, 2009). Years can pass between inundation events for individual playas, and hydroperiods depend on the soil type and the frequency and duration of rain events (Hillel, 2004; Gurdak and Roe, 2009). Water budget inputs to each playa basin include precipitation and runoff from surrounding topography, with outputs through either evapotranspiration or percolation downward through the playa base.

Recharge rates through playas can be controlled by rain flux, infiltration rate, K_{sat} and macropore fluid flux. At the beginning of rain events, the playa basin is dry, macropore flow (desiccation cracks) dominates, and the infiltration rate is controlled by the precipitation rate (Gurdak and Roe, 2009). During this period, macropores are open and can accept water at the precipitation rate as long as it doesn't exceed the soil infiltration rate (Gurdak and Roe, 2009). If rainfall is sufficient to cause the desiccation cracks to swell shut, the diffuse recharge

mechanism takes over (Gurdak and Roe, 2009). Hydric soils, like those in playa basins, shrink and swell with response to changes in water content (Gurdak and Roe, 2009). A study in Senegal measured a time of 4.5 hrs for desiccation cracks to close in a vertic soil, which would mark the transition from macropore to diffuse or focused recharge (Favre et al., 1997; Wilson, 2010). In instances when there is sufficient rainfall to inundate the playa with ponded water, infiltration is limited by the saturated hydraulic conductivity (K_{sat}) of the soil (Gurdak and Roe, 2009). Eventually, the ponded water will evaporate, transpire, or infiltrate, leaving a dry playa floor and allowing for desiccation cracks to reform (Gurdak and Roe, 2009).

Study Site

The Ehmke Playa site (38.4429, -100.6031), located on the CHP in Lane County, Kansas (Figure 2), was selected to investigate the hydrology of playas above the HPA. This location is ideal for measuring recharge to the HPA because the water table is shallow (11.5 m, all depths are reported as below ground surface, bgs, unless otherwise stated), and the land surface has not been affected significantly by anthropogenic modification. Area surrounding the playa has been left as rangeland with little/no intensive farming or irrigation influencing the playa or run-on water. Inflow to the playa basin is on the southwest end (Figure 3). The playa watershed is approximately 14 km^2 (5.4 mi^2), with the approximately 0.51 km^2 (0.20 mi^2) basin reaching a maximum depth of 0.75 m (2.5 ft) (Bowen and Johnson, 2012). A 1-km elongate aeolian dune, or lunette (Bowen et al., 2018), is located south-southeast of the playa basin (Figure 3).

The HPA underlying the study site consists of unconsolidated alluvial gravel, sand, silt and clay deposited to the east of the Rocky Mountains during the Miocene and Pliocene Epoch (Gutentag et al., 1984; Ludvigson et al., 2009). The alluvial sediments are often capped

with a hard caliche layer, which is overlain by aeolian fine sand, silt, and clay (Gutentag et al., 1984; Wood and Sanford, 1995). The aerial expanse of the entire HPA is approximately 450,000 km^2; the study site is located in the CHP, which encompasses approximately 125,000 km^2, or about 28% the expanse of the aquifer (Meixner et al., 2016). The climate in the CHP is semiarid, with potential evapotranspiration of 2,140 mm yr^{-1} and average precipitation of 505 mm yr^{-1} (High Plains Regional Climate Center, 2017; Meixner et al., 2016).

Methods

Soil Cores

Four soil cores were extracted with a Giddings soil coring machine from the playa center in June 2016, including EPC 1, 2, and 3 in the playa center to depths of 5.4 m (17.6 ft), 5.3 m (17.5 ft), and 5.3 m (17.4 ft), respectively; and EPC 4 on the south bench to depth of 7.3 m (24 ft) (Figure 3). Caliche prevented greater penetration depths in 2016, inhibiting sampling of the entire vadose zone. In August 2017, three additional soil cores were collected using an Acker hollow stem auger system, including EPC 5 and 6 in the playa center (completed to depths of 11.7 m (38.5 ft) and 8.2 m (27 ft), respectively), and EPC 7 in the interplaya to the north of the playa (completed to a depth of 16.8 m (55 ft)) (Figure 3). This second set of corings reached the water table in both locations, completely sampling the vadose zone. Soil cores were collected in 6 cm (2.4 in)-diameter, clear plastic core tubes of 0.9 m (3 ft)-length. The ends of the core tubes were capped and sealed with electrical tape (PVC) to prevent the loss of gases and moisture.

Vadose Zone Pore Water Analysis

Pore water chemistry was analyzed from four cores, including every 0.5 m from EPC 1 and 2, and every 1 m from EPC 5, and 7. Approximately 120 g of soil/sediment was used

for each sample, or between 3 and 5 cm length from a 6 cm diameter core. A 20 g aliquot was separated from each sample for measurement of field gravimetric water content (θ_{Gfield}), by oven drying at 105°C for 24 hrs. The volumetric water content (θ_{Vfield}) was estimated based on the volume of soil/sediment removed from the core and assuming a water density of 1 g mL^{-1}. The remaining 100 g of soil from each sample was air-dried in the controlled lab environment for 7 days and then re-weighed. Dried samples were softly ground using mortar and pestle to dis-aggregate clays. A saturated paste was then created using the air-dry soil and adding deionized (DI) water at a 1:1 ratio (Lindau and Spalding, 1984; Herbell and Spalding, 1993). Samples were then agitated for one minute, covered, and left for 24 hrs to ensure precipitated ions from pore water dissolved completely. Just before extraction, an aliquot of soil was removed for a second gravimetric water content (θ_{Gpaste}) measurement. Samples were then placed into extraction cups lined with two pieces of 2.7 µm filter paper (9.0 and 4.25 cm diameter), and placed onto a Model 24VE programmable vacuum extractor. Samples were left on the vacuum for 24 hours, resulting in extraction of 60 to 80 mL of pore water. The extracted pore water was then filtered using a syringe attached to a 0.45 µm attachable filter to remove sand and coarse silt from the sample. Afterwards, the specific conductance was measured using a Hach Waterproof Handheld meter to ensure the TDS was low enough to analyze using an Ion Chromatograph (IC). The meter was calibrated using solutions of 10 and 100 ppm. In instances of high TDS water, the sample was diluted with DI water prior to IC analysis. A 5 mL aliquot of each pore water sample was analyzed on the IC for fluoride, chloride, bromide, nitrate, and sulfate.

Instrument quantification limits (IQLs) were calculated using calibration curves with two high and two low standards for each anion. Two IC runs were completed, one in July

2017 and a second in August 2017. Calibration curves with plotted per anion per run using detector response as area under the curve along the x-axis and standard concentration along the y-axis (Figure A- 10 and Figure A- 11). A best-fit line was drawn on each of the calibration curves and the y-intercept, slope, and R^2 values calculated for each (Corley, 2003). The y-intercept and slope were then used to calculate the root mean square error (RMSE) and the R^2 value used to gauge validity of the best-fit line (Corley, 2003). The final IQLs were calculated as 10*RMSE divided by the slope (Corley, 2003). Then, the IQLs and R^2 values for both runs were averaged together, shown in Table A- 6. Results were output from the IC in mg L^{-1} (ppm). This value was converted to mg Kg^{-1} of dry soil using the following equation:

$$\frac{anion}{extracted\ water}\left(\frac{mg}{L}\right) \times\ \theta_{Gpaste}\left(\frac{g}{g}\right) \times \frac{1}{\rho_{water}}\left(\frac{mL}{g}\right) = \frac{anion}{soil}\left(\frac{mg}{Kg}\right) \qquad [1]$$

where θ_{Gpaste} is the gravimetric water content of the saturated paste described above and the density of water (ρ_{water}) is assumed 1 g mL^{-1}. The mg kg^{-1} concentration was then converted to mg L^{-1} of pore water using the following:

$$\frac{anion}{soil}\left(\frac{mg}{kg}\right) \times \frac{1}{\theta_{Gfield}}\left(\frac{g}{g}\right) = \frac{anion}{pore\ water}\left(\frac{mg}{L}\right) \qquad [2]$$

where θ_{Gfield}^{-1} is the inverse of the field gravimetric water content discussed above.

Chloride Mass Balance Method

The Chloride Mass Balance (CMB) method approximates recharge rates by comparing the concentration of chloride in the vadose zone system with the concentration of chloride input to the surface, with chloride assumed to move through the soil matrix at the same rate as infiltrating water. Chloride can be used as a conservative environmental tracer because it is non-volatile and

undergoes very little sorption or plant uptake (Scanlon, 1991). Sources of chloride are mainly from atmospherically transported material originating from the oceans, whereas inland areas likely have a more terrestrial source from weathering and erosion of clastic sediment (Davis et al., 1998). The CMB method is preferred over water balance calculations when measuring fluid recharge flux to aquifers in semiarid regions, where large evapotranspiration rates and inter-annual variations in precipitation result in a large error when calculating the typically small (<100 mm yr^{-1}) recharge rates (Scanlon, 1991). Inherent assumptions with the CMB method include constant rates of chloride deposition through time and a lack of horizontal flow in the vadose zone (Scanlon, 1991).

Four separate equations make up the CMB calculation. First, Equation 3 is used to determine the chloride wet and dry deposition at the land surface (q_{cl}) by multiplying the annual precipitation rate (P) by the chloride concentration in precipitation (Cl_p) (Allison and Hughes, 1978; Scanlon and Goldsmith, 1997):

$$q_{cl} = P \times Cl_p \quad [3]$$

The average (1952-2017) annual precipitation (505 mm) for the study site was obtained from a National Weather Service monitoring station in Scott City, Kansas, located approximately 26.8 km (16.7 mi) west of the study area (High Plains Regional Climate Center, CLIMOD, 2018). The concentration of chloride in precipitation (wet and dry) was measured in the SHP of Texas and New Mexico as 0.6 g m^{-3} (Nativ and Riggio, 1990) and utilized in subsequent CMB calculations in two Texas studies (Wood and Sanford, 1995; Scanlon and Goldsmith, 1997). The annual rainfall rates for the two Texas studies (485 mm, Wood and Sanford, 1995; 500 mm, Scanlon and Goldsmith, 1997) are similar to that at the Ehmke Playa site (505 mm) and the value of 0.6 g m^{-3} for Cl_p is assumed reasonable for the study site. Using Equation 3, the q_{cl} is calculated as 0.3 g m^{-}

^{2}. A recent study in northwest Kansas with similar average annual precipitation (485 mm) also used a q_{cl} value of 0.3 g m^{-2} for CMB calculations (Katz et al., 2016).

Next, the fluid flux rate through the vadose zone (q) is calculated by dividing the q_{cl} from Equation 4 by the chloride concentration in the unsaturated zone (Cl_{uz}) (Allison and Hughes, 1978; Scanlon and Goldsmith, 1997):

$$q_1 = q_{Cl}/Cl_{uz} \quad [4]$$

Equation 4 assumes that the only source of chloride deposition is from wet and dry precipitation into the playa; however, playas are closed basins and will often have additional chloride mass from run-off water in the surrounding watershed. By underrepresenting the total amount of chloride deposition in the playa basin, Equation 4 may cause inaccuracies, such as an underestimation of the fluid flux. To account for chloride in run-off water into a playa, the following equation was developed (Wood and Sanford, 1995; Scanlon and Goldsmith, 1997):

$$q_2 = \frac{P \times Cl_p}{Cl_{uz}} + R\frac{A_b \times Cl_r}{A_f \times Cl_{uz}} \quad [5]$$

where R is runoff, A_b is the area of the watershed (14 km^2), A_f is the area of the playa (0.51 km^2), and Cl_r is the concentration of chloride in the run-off water. The Cl_r is assumed the same as Cl_p at this site, or 0.6 g m^{-3} because there are not sufficient quantities of chloride sources in surficial sediments to alter the concentration in run-off water.

If chloride vadose zone profiles are collected in differing years, the fluid flux can be estimated based on the chloride peak displacement depth and time elapsed between the two measurements. This third flux equation is shown below (Stonestrom et al., 2003; McMahon et al., 2006; Gurdak et al., 2007):

$$q_3 = \frac{\theta_{\text{Vfield}}(z_2 - z_1)}{(t_2 - t_1)} \quad [6]$$

where θ_{Vfield} is the volumetric water content of the specified core between the two chloride peaks, z_2 and z_1 are the depths of chloride peaks, and t_2 and t_1 are the corresponding times of measurement.

After calculating a fluid flux based on Equation 4, 5, or 6, a simple travel time through the vadose zone can be calculated by Equation 7 below:

$$\text{tt}_1 = \text{z}_{\text{wt}}/\text{q} \quad [7]$$

where z_{wt} is depth to the water table and q is the calculated fluid flux. Additionally, a second travel time calculation can be used by averaging the volumetric mass of chloride in a depth interval and dividing by the chloride land deposition (Wood and Sanford, 1995; Scanlon and Goldsmith, 1997):

$$tt_2 = \frac{\int_0^z \theta_{vfield} Cl_{uz} dz}{q_{cl}} \quad [8]$$

where the θ_{Vfield} is the field volumetric water content of the sample.

Groundwater

Three monitoring wells were installed at the study site in June 2016, including well 1 in the playa center, well 2 southeast of the lunette, and well 3 to the southwest of the playa near the inflow (Figure 3). Well 1 was drilled to a total depth of 31.5 m (103.4 ft), well 2 to 30.1 m (98.8 ft), and well 3 to 30.0 m (98.3 ft) (all depths are reported as below ground surface, unless otherwise stated). Surface elevations were extracted from LIDAR using coordinates and are 867.8 m (2,847.2 ft) above mean sea level (amsl), 871.6 m (2,859.6 ft)

amsl, and 874.2 m (2,868.0 ft) amsl at wells 1, 2, and 3, respectively. Each well was instrumented with a Solinst Levellogger pressure transducer, allowing for hourly water level measurements. A Solinst Barologger was placed in well 1 at 6.4 m (21 ft) below top of casing for barometric pressure corrections (Figure 3). Water level measurements were downloaded on a biannual basis in June and July of 2016 and June and August of 2017 and range from 11.47 to 11.55 m (37.6 to 37.9 ft) in the playa and 15.97 to 16.50 m (52.4 to 54.1 ft) in the interplaya (all depths are reported as below ground surface, unless otherwise stated). Groundwater elevations were calculated at the site from the August 2017 sampling event in well 1 (856.4 m amsl, 2,809.6 ft amsl), well 2 (855.6 m amsl, 2,807.0 ft amsl) and well 3 (857.7 m amsl, 2,814.0 ft amsl) (Figure 3). Using the HydrogeoEstimatorXL tool (Devlin and Schillig, 2017), groundwater at the Ehmke Playa site is flowing under a hydraulic gradient of 0.0016 towards north 66° east.

In August 2017, groundwater samples were collected from the three monitoring wells installed for this project, as well as an existing windmill located near the playa (Figure 3). Samples were collected using a 1-m long Solinst stainless steel discrete interval sampler and stored in 100 mL polyethylene bottles with limited headspace. Anion concentrations were analyzed determined using IC, similar to the pore water samples.

Vadose Zone Matric Potential

Matric Potential (MP) is a function of both capillary pressure and adsorption of water, and arises from the attraction of water to the surface of soil particles (Scanlon and Goldsmith, 1997). This is measured at the Ehmke Playa site via dielectric water potential sensors, which utilize a ceramic disc with a known moisture characteristic curve. The sensor measures the gravimetric water content of the ceramic disc and matches the appropriate MP from the curve. Because the MP

measures the potential energy in the vadose zone, measurements are either negative or zero. Values of near zero represent saturated conditions; as values become increasingly negative, soil conditions become increasingly dry.

In June 2016, a pit was excavated in the approximate center of the playa just south of well 1 to 2.4 m (8 ft) for installation of dielectric water potential sensors (MPS-6 by Decagon Devices, Inc.) at depths of 0.12 m (0.39 ft, sensor 1), 0.47 m (1.54 ft, sensor 2), 0.96 m (3.14 ft, sensor 3), and 1.52 m (4.99 ft, sensor 4). These sensors were connected to a Campbell Scientific data logger and programmed for hourly monitoring of vadose zone MP and soil temperature. The instrument detection limit ranges from -9 to -100,000 kPa for MP and from -40 to 60°C for soil temperature. Additionally, a weather station at the center of the playa monitors wind, temperature, precipitation, barometric pressure, and net radiation, with photographs taken twice daily by a Campbell CC5MPX digital network camera. From the pictures, it was deduced that the playa was inundated with water from April 13 through May 16, 2017. Prior to this rain event, the playa had not been completely inundated to the annulus, or rim of the basin, for 2 to 3 yrs (Vance and Louise Ehmke, Personal Communication).

MP sensors were utilized to supplement data from the anion depth profiles and CMB calculations, and provide information on saturation in the upper soil and sediment. It has been hypothesized that the CMB method represents only interstitial flow (diffuse) and thereby does not sufficiently represent recharge through macropores (Wood, 1997). MP sensors can support data identified in the CMB by measuring pulses of water saturation, which includes water movement through both interstitial space and macropores.

Particle Size Analysis

Particle size analysis was completed using a Malvern Mastersizer 2000 laser diffraction system to identify texture in EPC 4 and in the instrumented pit at the playa center. Samples were collected every 2 to 4 cm in EPC 4 to a depth of 7.25 m and every 5 cm to a depth of 2.35 m in the instrumented pit. Each sample was packed into 8 cm^3 plastic cubes and dried for 48 hrs at 60°C. After drying, rootlets were removed and the sediment pulverized, submerged in de-ionized water, and then sonicated for 3 minutes. Malvern analysis reported each sample texure as a percentage of clay, silt and sand.

Infiltrometer

In August 2017, a Decagon Devices DualHead Infiltrometer was used to measure the K_{sat} of the surface soil at four locations. Two measurements were collected at the playa center (Inf 1 and 2) near EPC 1 and two measurements were collected at the interplaya (Inf 3 and 4) near EPC 7 (Figure 3). The infiltrometer uses an encased pressurized chamber filled with water to maintain a constant pressure head through a series of high and low pressure cycles. A soak time of 25 minutes was chosen to properly wet the soil, followed by three pressure cycles using a high-pressure head of 15 cm and a low-pressure head of 5 cm. Following the pressure cycles, K_{sat} is calculated by averaging the result of the three cycles.

Hydrus-1D Model

The Hydrus-1D Software Package was utilized to constrain fluid flux rates in the vadose zone calculated both via CMB method and MP measurements (Šimůnek et al., 2013). The model was run for 169 days based on the precipitation data from December 2016 through June 2017. The upper boundary condition is the measured precipitation at the site and the lower boundary condition is a constant pressure head (11.5 m) to represent the water table.

Texture from EPC 4 was input into the model, and an initial condition for MP was input as -8,000 kPa. Four nodes (0.4, 1.6, 5.1, and 11.5 m) were placed through the depth of the model for estimation of fluxes through time.

Results and Discussion

Anion Sources

Sources of anions in pore water and groundwater include atmospheric precipitation, anthropogenic influence, and weathering of soil, rocks, and minerals. Aerosols from coastal regions are rich in certain anions (chloride, bromide, sulfate and to a lesser degree fluoride) and are easily transported with rain events (Herczeg and Edmunds, 2000; Scanlon et al., 2009). Because these ions have a marine source, their concentrations in precipitation are typically higher in coastal areas and lower in mid-continent areas such as Kansas. In addition to marine aerosols, weathering of minerals and rocks also has an effect on ions in meteoric precipitation. Chloride and bromide mineral sources include dissolution of marine rocks like halite; sulfate from dissolution of gypsum, anhydrite, and pyrite; and fluoride from dissolution of fluorite and apatite (Scanlon et al., 2009; Katz et al., 2016). Articulating nitrate sources is slightly more complicated because nitrogen can exist as various species (atmospheric nitrogen, nitrate, nitrite, and ammonia), which are biologically used by flora and fauna through the nitrogen cycle. In addition to natural sources, there are also anthropogenic sources of nitrate, sulfate, and fluoride from manufacturing and fertilizer application.

The sorptivity of ions, or the ability to sorb on to soil surfaces, relates to their mobility. Fluoride and sulfate have the highest sorptivity of the anions examined and they move more slowly through the vadose zone than chloride (Scanlon et al., 2009). Bromide and chloride

have fairly low sorptivity and thereby move conservatively through the vadose zone with minimal sorption (Scanlon et al., 2009). Nitrate has a lower sorptivity than chloride but does not act conservatively due to biological interference discussed above (Scanlon et al., 2009).

Chloride and Water Content in the Vadose Zone

The gravimetric water content in the playa (EPC 1, 2 and 5) ranges from 0.05 to 0.24 g g^{-1}. In the interplaya vadose zone (EPC 7) the gravimetric water content was between 0.11 and 0.16 g g^{-1} (Figure 4). Volumetric water contents were similar in both the playa (0.10 to 0.33) and the interplaya (0.15 to 0.34) (Table 1 and 2).

Water-extractable chloride concentrations ranged from 12 to 140 mg L^{-1} in the three playa cores (EPC 1, 2, and 5), and from 301 to 3,900 mg L^{-1} in the interplaya (EPC 7) (Table 1 and 2). The playa chloride profile has several small peaks at 2, 5, and 9 m; each peak has a different magnitude in each core. For example, the 2 m peak is smaller in core 2 (25 mg L^{-1}) and core 5 (37 mg L^{-1}) than it is in core 1 (140 mg L^{-1}) (Figure 4). The interplaya core exhibits one maximum peak at 2 m (3,900 mg L^{-1}), and then gradually decreases in concentration to around 34 mg L^{-1} to the water table (16.7 m).

Vadose zone water-extractable chloride concentrations and field gravimetric contents show trends for and plant transpiration in the root zone and flushing in 2017. A dip in gravimetric water content occurs at 2 m in all four cores (0.05 to 0.16 g g^{-1} in playa, 0.13 g g^{-1} in interplaya), dropping from a peak at around 1 m (0.14 to 0.21 g g^{-1} in the playa, 0.15 g g^{-1} in the interplaya) (Figure 4). Maximum chloride concentrations in EPC 1 (140 mg L^{-1}) and EPC 7 (3,900 mg L^{-1}) also occur at 2 m. Combined, the low gravimetric water contents and high chloride concentrations are indicative of water removal by plants at this depth via transpiration (Scanlon, 1991). EPC 1 (0.05 to 0.24 g g^{-1}) and 2 (0.12 to 0.22 g g^{-1}) have lower

gravimetric water contents than EPC 5 (0.16 to 0.24 g g^{-1}) in the upper 5 m, which indicates water movement through the profile between 2016 and 2017. The lowest gravimetric water content in EPC 5 (0.06 g g^{-1}) is at 9 m, which may represent the depth of flushing or could be due to textural changes.

A similar inverse relationship between chloride concentrations and gravimetric water content is observed throughout much, but not all, of the cores. In the complete playa core (EPC 5), two chloride peaks exist at 5 m (46 mg L^{-1}) and 9 m (72 mg L^{-1}), with corresponding gravimetric water contents of 0.24 g g^{-1} and 0.06 g g^{-1}, respectively (Figure 4). The maximum chloride concentration at 9 m corresponds to the lowest measured gravimetric water content; however, the 5 m chloride peak corresponds to a high gravimetric water content. It is expected that high chloride concentrations would correlate with low water contents, as seen at 9 m, due to the inverse relationship between chloride concentrations and fluid recharge flux. However, water content may be more closely related to texture than ion concentration. Malvern results from EPC 4 show coarser textures with depth increasing from an average sand content of 5% (upper 5 m) to 27% (5 to 7.24 m), which suggests that the lower water contents at 9 m relative to 5 m beneath the playa is due to coarser textures at depths near the water table (Figure 10).

Although chloride concentrations peak at 2 m in the playa (EPC 1) and interplaya (EPC 7) cores, the magnitude is vastly different. The appreciably higher interplaya concentration is evidence that water is traveling more slowly, allowing for accumulation of chloride over a long period of time. Although evapoconcentration is also evident in the playa, the smaller magnitude implies a shorter timeframe for chloride accrual. Salt concentration at the base of the root zone is common in semiarid regions due to transpiration by plants (Scanlon, 1991). In addition, the shape of the interplaya chloride profile could have implications for long-term

climate variations (Allison and Barnes, 1985; Scanlon, 1991). Over long time periods, the transition from a wetter climate during the early Holocene (high fluid flux) to a drier climate in the middle and late Holocene (low fluid flux) could result in lower chloride concentrations in the lower profile and higher chloride concentrations in the upper profile (Scanlon, 1991).

Other Anion Concentrations in the Vadose Zone

Concentrations of other anions, including bromide, sulfate, fluoride, and nitrate, have similar patterns through the vadose zone. All anion concentrations have a higher maximum in the interplaya than the playa, indicating fluid flux through the playa is higher, with longer ion residence times beneath the interplaya. Bromide concentrations ranged from <0.1 to 6.5 mg L^{-1} in the playa and from <0.1 to 18 mg L^{-1} in the interplaya (Table 1, and Table 2). Although all were completed in the playa center, EPC 5 did not contain bromide at concentrations above the IQL, whereas EPC 1 (5.4 mg L^{-1}) and 2 (6.5 mg L^{-1}) contained detectable bromide with a maximum peak occurring at the surface (Figure 4). Nitrate-N concentrations ranged from <0.2 to 3.4 mg L^{-1} in the playa, and from <0.2 to 7.6 mg L^{-1} in the interplaya. Sulfate concentrations ranged from 58 to 450 mg L^{-1} in the playa and from 59 to 2,600 mg L^{-1} in the interplaya. Fluoride concentrations ranged from <0.2 to 60 mg L^{-1} in the playa, and from 4.0 to 66 mg L^{-1} in the interplaya.

Similar to chloride, two other anion concentration peaks are found at 2 m beneath the interplaya, including bromide (18 mg L^{-1}) and sulfate (2,600 mg L^{-1}), while fluoride exhibits a minima (4.0 mg L^{-1}) and nitrate (<0.2 mg L^{-1}) a low value at 2 m (Figure 4). Bromide, sulfate, and chloride are all expected to peak at 2 m due to long term evapoconcentration of salts in the root zone via transpiration by plants, and/or from paleoclimatic influence. The reason for low values of nitrate and fluoride in the interplaya at this depth could be due to

plant uptake of these nutrients; although fluoride is not an essential plant nutrient, it can still undergo plant uptake (Scanlon et al., 2009).

In contrast, playa anion depth profiles are variable, with some concentration peaks at 2 m, but others at the surface or deeper in the profile. The only playa core that exhibits a large sulfate peak at 2 m is EPC 1 (360 mg L^{-1}), whereas EPC 2 (130 mg L^{-1}) and 5 (110 mg L^{-1}) exhibit smaller peaks at this depth. Sulfate concentration maxima in EPC 1, 2, and 5 occur at 0.25 m (450 mg L^{-1}), 0.25 m (370 mg L^{-1}), and 5 m (330 mg L^{-1}), respectively. A high concentration of sulfate may also exist at 0.25 m in EPC 5, but the first sample was collected at 0.5 m (110 mg L^{-1}). Peak bromide concentrations in both EPC 1 and 2 (5.4 mg L^{-1} and 6.5 mg L^{-1}, respectively) were observed at the surface, and all bromide concentrations for EPC 5 were <0.1 mg L^{-1}. Fluoride concentrations in the playa peak at 0.77 m, 2 m and 4.7 m in EPC 1 (14 mg L^{-1}), 1.7 m and 4.1 m in EPC 2 (16 mg L^{-1}), and 9 m in EPC 5 (60 mg L^{-1}). Nitrate concentrations are below the IQL in EPC 1, peak at 5 m in EPC 1 (0.83 mg L^{-1}), and peak at 9 m in EPC 5 (3.4 mg L^{-1}) (Figure 4). These data suggest evapoconcentration at 2 m is affecting playa chloride, sulfate, and fluoride concentrations in EPC 1 and chloride concentrations in EPC 2. Contrarily, EPC 5 does not contain any anion maxima at the 2 m depth and instead they occur deeper in the profile at 5 or 9 m.

The anion concentration variability in the playa center is likely due to differences in antecedent conditions for the two coring periods roughly a year apart. EPC 1 and 2 were sampled in 2016, when the playa had not been inundated to the annulus for 2 to 3 yrs. From April 13 to May 16, 2017, the playa was inundated to the annulus, then the water evaporated, transpired, and percolated prior to the collection of EPC 5 in August, 2017. Bromide was not detected above the IQL in playa core EPC 5, while EPC 1 and 2 have concentrations ranging

from <0.1 to 6.5 mg L^{-1} (Figure 6). The lack of measureable bromide in EPC 5 could be from flushing of salts during the 2017 inundation event, or increased water content diluting bromide concentrations below the IQL. Deeper concentration peaks at 5 m for sulfate (330 mg L^{-1}) and 9 m for chloride (72 mg L^{-1}) fluoride (60 mg L^{-1}), and nitrate (3.4 mg L^{-1}) provide additional evidence for flushing in EPC 5. These may represent the depths of flushing, as chloride also has a second smaller peak at 5 m (46 mg L^{-1}), as discussed above. Sulfate movement could be slower due to higher sorptivity resulting in shallower flushing depths when compared to chloride, fluoride, and nitrate. Similar to EPC 5, EPC 1 and 2 also exhibit chloride and sulfate peaks at 5 m, but it is unknown if peaks exist deeper in the profile. The overall differences observed in the playa could represent intrinsic variability in pore water anion concentrations, or could be influenced by the smaller sampling interval in EPC 1 and 2 (every 0.5 m) than EPC 5 (every 1 m). The variation in chloride concentrations in EPC 1 and 2 likely constrain these values when the playa has not been inundated for 2 to 3 years. Nonetheless, lower concentrations of anions in the upper 5 m and deeper concentration peaks in EPC 5 when compared to EPC 1 and 2 may be evidence of flushing during 2017 and mobilization of ions downwards into the profile. The pattern of peak anion concentrations at 2 m is not as consistent in the playa core as in the interplaya core, and is not observed in the second set of playa cores, suggesting more frequent flushing in the playa than the interplaya.

Vadose zone ratios for bromide/chloride, nitrate/chloride, sulfate/chloride, and fluoride/chloride range from 0.023 to 0.20, 0.014 to 0.064, 0.92 to 16, and 0 to 1.1, respectively in the playa and from 0.004 to 0.0059, 0.0024 to 0.016, 0.67 to 4.9, and 0.0010 to 1.2, respectively in the interplaya (Table 3, Table 4, and Figure 7). Sulfate is the only anion measured with concentrations up to 15 times higher than chloride concentrations, a relationship observed only in

the playa. It is possible that sulfate accumulates relative to chloride beneath the playa due to preferential chloride flushing and sorption of sulfate.

When anion mass ratios (mg L^{-1}) are compared with chloride concentration (mg L^{-1}), conclusions can be drawn about the sources of salinity (Figure A- 8 and A-9). Interestingly, the EPC 7 samples have nearly constant ratios at high chloride concentrations, implying evapoconcentration is occurring causing mineral precipitation (Whittemore, 1995). As the interplaya vadose zone becomes increasingly dry from evapotranspiration, it is possible that halite and gypsum may be precipitating in the root zone and subsequently re-dissolving when rain events saturate the upper soil. Ratios are higher and chloride concentrations are lower in the playa than the interplaya suggesting more frequent flushing in the playa.

Linear regression analysis provides insight into relationships among anion concentrations in the playa and interplaya. In EPC 1 and 2, the only anions that appear somewhat positively correlated are sulfate and chloride with an R^2 value of 0.65 and 0.81, respectively (Figure A- 1 and A-2). In EPC 5 this trend is not repeated, sulfate and chloride have an R^2 value of 0.01, and the best-fit line has a slightly negative slope (Figure A- 3). This temporal change between the 2016 and 2017 cores supports the idea of preferential chloride flushing during the 2017 inundation event, changing the sulfate/chloride ratios and resulting in the slightly negative slope of the best-fit line.

Anions in the interplaya are better correlated than those in the playa, with R^2 values of 0.99 for bromide and chloride, 0.90 for sulfate and chloride, and 0.90 for sulfate and bromide (Figure A- 4). Possible reasons for high correlations in these three anions is the nature of interplaya recharge flux. Interplaya recharge occurs during rain events and consists of small plugs of water moving through the vadose zone. These smaller recharge events do not result in a significant subsurface pulse, and provide the ions a longer timeframe to equilibrate with the concentration of

ions already present in the vadose zone. With playa recharge events happening largely through focused flow and macropore recharge, more conservative ions (chloride, bromide) are preferentially flushed, reducing the correlation and lowering R^2 values (lower correlations).

Studies of playas in the SHP exhibit similar chloride concentration patterns, where much lower concentrations are observed in playas than adjacent interplaya areas. In the Texas SHP, playa and interplaya chloride concentrations range from 0.3 to 451 mg L^{-1} and 55 to 19,293 mg L^{-1}, respectively (Table 9) (Wood and Sanford, 1995; Scanlon and Goldsmith, 1997; Wood, 1997). This is consistent with the magnitude difference seen between the playa and interplaya areas (12 to 140 mg L^{-1} and 31 to 3,900 mg L^{-1}, respectively) at the Ehmke Playa site. Chloride vadose zone inventories were also measured in the NHP and CHP in rangeland and irrigated cropland. Concentrations measured in rangeland have a maxima of 42 mg kg^{-1} and in irrigated cropland of 65 mg kg^{-1} (Table 10) (McMahon et al., 2006; Gurdak et al., 2007; Katz et al., 2016). These values are slightly elevated when compared to the chloride concentrations measured beneath the playa during this study (2.9 to 11 mg kg^{-1}), but are much lower than those measured at the interplaya (4.0 to 490 mg kg^{-1}).

When compared to SHP and CHP sites, the Ehmke Playa site has low sulfate and nitrate concentrations and elevated fluoride and bromide concentrations. Sulfate depth-weighted average concentrations (Table 9) measured beneath 2 sites in Texas SHP rangeland (2,500 to 7,700 mg L^{-1}, Scanlon et al., 2009) are higher than the depth-weighted sulfate average observed in this study's interplaya core (EPC 7, 540 mg L^{-1}). Beneath 15 sites in SHP rain-fed cropland, sulfate depth-weighted average concentrations vary (71 to 5,000 mg L^{-1}, Scanlon et al., 2009), with lower values comparable to the Ehmke Playa site (130 mg L^{-1} in EPC 5, 480 mg L^{-1} in EPC 7, Table 5). SHP fluoride depth-weighted average concentrations

measured beneath rangeland (80 to 87 mg L^{-1}) are similar to those beneath rain fed agriculture (35 to 77 mg L^{-1}) (Scanlon et al., 2009), and slightly elevated when compared to those at the Ehmke Playa site (24 mg L^{-1} in EPC 5, 35 mg L^{-1} in EPC 7). In the SHP, fluoride was not mobilized by flushing from land-use changes (Scanlon et al., 2009); which could explain the similar playa and interplaya concentrations in this study. Bromide concentrations detected in the playa (maxima of 0.78 mg kg^{-1}) and interplaya (maxima of 2.2 mg kg^{-1}) at the field site (Table A- 2 and Table A- 3) are elevated compared to a nearby Kansas NHP study site beneath an irrigated field (maxima of 0.2 mg kg^{-1}) (Katz et al., 2016). Contrarily, nitrate concentrations are quite low beneath the study site playa (maxima of 0.39 mg kg^{-1}) and interplaya (maxima of 1.2 mg kg^{-1}) when compared to CHP rangeland (maxima: 80 to 290 mg kg^{-1}) and irrigated sites (maxima: 15 to 55 mg kg^{-1}) (McMahon et al., 2006; Gurdak et al., 2007; Katz et al., 2016). Elevated levels of nitrate in vadose zones under irrigated agriculture are likely due to application of fertilizers.

Chloride Mass Balance

Fluid flux rates through the vadose zone were calculated using three different equations (Equations 4, 5, and 6). The first method (Equation 4) assumes the only input of chloride to the system is via wet and dry deposition, giving depth-weighted flux rates between 8 and 15 mm yr^{-1} in the playa and 4 mm yr^{-1} in the interplaya. The fluid flux through the playa using this method is likely an underestimation because additional chloride mass from watershed run-off is ignored (Flint et al., 2002). Therefore, the calculated travel times from Equation 7 utilizing these flux rates (1,400 yrs to 11.5 m) likely represent maxima for the playa. The calculated travel time of 4,800 years for the interplaya is expected as the only chloride source

in this location is from direct precipitation. Additionally, the second calculated interplaya travel time (5,500 yrs) from Equation 8 is comparable.

Equation 6, which compensates for the chloride mass from the surrounding runoff, was calculated using values for R of 5% (25.3 mm yr^{-1}), 10% (50.1 mm yr^{-1}), and 20% (101 mm yr^{-1}) of annual precipitation. Fluid fluxes calculated for the playa and a value of R as 5%, 10%, and 20% of annual precipitation, range from 20 to 37 mm yr^{-1}, 31 to 58 mm yr^{-1}, and 54 to 100 mm yr^{-1}, respectively (Table 11). Travel times (Equation 7) to 11.5 m are 580, 370, and 210 yrs to corresponding R values of 5%, 10%, and 20%, respectively. Scanlon and Goldsmith (1997) estimated that run-off water to basins in the SHP accounted for approximately 10% of annual precipitation in a watershed of fine-grained texture, which is modified from Wood and Sanford (1995) who used a R value of 5% in a coarse-textured soil. The 10% value for R is likely the most representative of this study area because the watershed surface soil is silty clay loam and the annual precipitation (505 mm) is similar to that used in by Scanlon and Goldsmith (1997) (500 mm). However, the CHP experiences inter-annual variations in precipitation (370 to 845 mm) and higher values for R may be more representative of wetter years.

Oddly, travel time calculations from Equation 8 in the playa are shorter in the pre-inundation cores (EPC 1 and 2, 2016) than the post-inundation core (EPC 5, 2017). In EPC 5, travel times calculated to 5 m is 170 yrs, but in EPC 1 and 2 is 92 and 84 yrs, respectively. It would be expected that post-inundation travel times would be faster due to flushing. Reasons for this discrepancy could be from the higher depth-weighted averages in EPC 5 for θ_{Vfield} and Cl_{uz} than in EPC 1 and 2, as Equation 8 is directly related to these two variables.

The only flux calculation that takes into account temporal displacement of peak chloride values is Equation 6. EPC 1 (June, 2016) has a chloride peak at 2 m and EPC 5 (August, 2017) has a chloride peak at 9 m. As an inundation flushing event occurred between collection of these two cores (April 13 to May 16, 2017), fluid fluxes can be estimated for dry periods without inundation from EPC 1 and for wet periods during/ after inundation from EPC 5. The first flux calculated for EPC 1 utilizes a depth-weighted θ_{Vfield} of 0.12 measured from the surface to 2 m. With an inundation event every occurring every 2 to 3 years, the flux rate from EPC 1 is between 78 and 118 mm yr^{-1}, equating to a travel time to the aquifer of 100 to 150 yrs. For the second fluid flux calculated from EPC 5, a depth-weighted average θ_{Vfield} of 0.28 measured from 2 to 9 m was used, along with a 1.17 yr timeframe between the two core sampling events. The 2017 fluid flux was calculated as 1,700 mm yr^{-1}, which calculates to a travel time to the aquifer of 8 yrs. These travel times suggest faster movement during inundation periods and exceed those estimated by previous equations.

Calculated fluid fluxes through the vadose zone to the HPA in the playa are higher by at least one order of magnitude than those for the interplaya, which compares well to playa studies in the SHP. In the SHP, playa and interplaya fluid fluxes range from 60 to 100 mm yr^{-1} and from 0.1 to 4 mm yr^{-1}, respectively (Wood and Sanford, 1995; Scanlon and Goldsmith, 1997), compared with fluids fluxes from the Ehmke playa and interplaya of 78 to 118 mm yr^{-1} and 0.1 to 10 mm yr^{-1}, respectively. Despite this similarity, a study by Wood et al. (1997) indicates total fluid flux through SHP playas is actually much higher (750 to 2,720 mm yr^{-1}), suggesting the CMB method measures only the interstitial fluid flux (22 to 34 mm yr^{-1}) while ignoring macropore fluid flux (Table 9). There is currently disagreement over whether the CMB method calculates interstitial recharge and ignore macropore recharge, or represents the

total system recharge (Wood, 1997; Scanlon, 1999). Nonetheless, these higher recharge rates calculated by Wood et al. (1997) are similar to that calculated via Equation 6 with the 2017 core (1,700 mm yr^{-1}) and may represent higher playa fluid flux during inundation periods. Wood et al. (1997) also estimated that 84% of the SHP regional recharge (11 mm yr^{-1}) occurs through playa macropores. Similarly high inundation infiltration rates were measured in the SHP by Ganesan et al. (2016) through playas surrounded by both grassland (320 to 1,700 mm yr^{-1}) and cropland (730 to 7,200 mm yr^{-1}) watersheds.

Fluid flux rates through CHP and nearby NHP rangeland (0.2 to 5 mm yr^{-1}) and irrigated cropland (39 to 138 mm yr^{-1}) (Table 10) (McMahon et al., 2006; Gurdak et al., 2007; Katz et al., 2016) compare well to study site interplaya (0.1 to 10 mm yr^{-1}) and playa (78 to 118 mm yr^{-1}). Gurdak et al., (2007) also measured total recharge (196 to 390 mm yr^{-1}) irrigated agriculture by correlating groundwater level responses to precipitation events; this is slightly elevated when compared to Equation 6 from EPC 1 (78 to 118 mm yr^{-1}), but much lower than that estimated during/ after inundation (1,700 mm yr^{-1}). Interplaya water flux rates from the study site (0.1 to 10 mm yr^{-1}) are consistent with regional recharge estimates for regional recharge from Kansas (4 to 18 mm yr^{-1}) (Katz et al., 2016; Meixner et al., 2016).

Vadose zone travel times calculated at the study site compared well to other studies completed beneath the NHP, CHP and SHP. In the CHP, travel times beneath rangeland and irrigated cropland to the water table (50 m and 45 m, respectively) were calculated at 2000 yrs, and between 49 to 130 yrs, respectively (Table 10) (McMahon et al., 2006; Gurdak et al., 2007). Katz et al. (2016) also measured a travel time of 45 yrs to a depth of 36 m at an irrigated site in northwestern Kansas. Travel times through the playa (100 to 150 yrs) are slightly elevated with respect to these CHP studies; however, the inundation travel time of 8 yrs is

elevated when compared to CHP rangeland and irrigated cropland (Table 11). The travel times to 16.7 m measured in the interplaya (4,800 to 5,500 yrs) are elevated to those in CHP rangeland, but are within the measured range for three SHP interplaya sites (5,000 to 9,900 yrs) with 4.5 to 26.3 m thick vadose zones (Scanlon and Goldsmith, 1997).

Groundwater

Anion concentrations from the four groundwater wells were fairly similar and ranged from 20 to 26 mg L^{-1} for chloride, <0.1 to 0.20 mg L^{-1} for bromide, 1.0 to 1.5 mg L^{-1} for nitrate-N, 48 to 82 mg L^{-1} for sulfate, and 1.8 to 2.9 mg L^{-1} for fluoride (Table 7). The upgradient well (well 3) exhibited the highest concentrations for chloride, nitrate, sulfate, and fluoride. Conversely, the east windmill well exhibited the lowest concentrations for chloride, nitrate, sulfate, and fluoride. Bromide was the only anion that did not follow this trend, with the highest concentration in the east windmill well and the lowest concentration in the playa center (well 1). Ratios of bromide/chloride in groundwater wells range from 0.0040 to 0.010 (Table 8).

Groundwater ratios of bromide/chloride can be used to identify sources of groundwater and ranged from 0.0040 to 0.010 at the study site. Higher ratios between 0.007 and 0.02 are indicative of atmospheric precipitation and lower ratios between 0.005 to 0.01 are indicative of shallow groundwater (Whittemore, 1995; Davis et al., 1998). The higher ratios were measured in the downgradient sample (east windmill well, 0.010). Lower bromide/chloride ratios were measured in upgradient well 3 (0.0040) and in downgradient well 2 (0.0058) (Table 8). In well 1, bromide was below the IQL (<0.1) meaning that the ratio is low (<0.0048). In South-Central Kansas, lower bromide/chloride ratios (0.02 to 0.007) indicate meteoric precipitation is the main chloride source, but with minor influences from other

sources including salt dissolution, upgradient water, or evaporation (Whittemore, 1993; Davis et al., 1998). This suggests an influence outside of meteoric precipitation for hydraulically upgradient groundwater (minor salt dissolution, evaporation), whereas the east windmill well suggests only a meteoric influence. A possible reason for higher bromide/chloride ratio in hydraulically downgradient waters is from meteoric influence at the playa.

Anion bromide/chloride and sulfate/chloride in groundwater are plotted against chloride concentration and compared to those in the vadose zone. Bromide/chloride ratios in groundwater are similar to those in EPC 7, but chloride concentrations are much lower (Figure A- 8). The similarity of bromide/chloride ratios in EPC 7 and groundwater support the idea that ions in the interplaya vadose zone are equilibrating with the incoming ions from precipitation and suggests minor quantity of recharge. Contrarily, bromide/chloride ratios and chloride concentrations in groundwater are lower than those measured in EPC 1 and 2. The higher bromide/chloride ratio in playa cores suggests more sufficient influence from meteoric precipitation. Bromide/chloride ratios in groundwater are comparable to those measured by Whittemore (1995) in the Prairie Bend Aquifer in south-central Kansas. Sulfate/chloride ratios in groundwater are comparable to those measured in EPC 5 (Figure A- 9). As EPC 5 doesn't show much evidence of evapoconcentration (as do EPC 1 and 2), the similarity to groundwater samples may suggest that evapoconcentrated ions have been flushed by meteoric precipitation creating similar sulfate/chloride ratios and chloride concentrations to groundwater.

Matric Potential

MP was measured at four soil depths from December 2016 to June 2017. During the winter months, MP was very negative (<-6,000 kPa) throughout all installed depths (12, 47,

96, and 152 cm) (Figure 11). Beginning in on February 19, MP values at sensor 1 (12 cm) began to increase, although remained quite negative until March 29. During this time, through a series of pulses, the MP increased nineteen times. Individual pulses lasted for long periods of time (10 hrs to 6.8 days), with MP increasing from -7,999 kPa to a range between -6,413 kPa and -1,524. On March 29 at 11:30 AM, the MP increased above field capacity (FC), remaining at this higher potential throughout the remainder of the observation period (June 12). The increase in MP past FC is attributed to rain, which totaled 56.9 mm from March 23 at 8:00 PM to March 29 at 11:30 AM. The most significant rain events occurred on March 23 (12.5 mm), March 28 (35.8 mm) and March 29 (7.9 mm). These were the first significant precipitation events of the study, with only a total of 19.05 mm of rain falling between December 26 at 11:20 AM and March 23 at 8:00 PM.

The second sensor (47 cm) recorded very negative MP (-7,999 kPa) until April 11 at 11:20 AM, when the MP begins to pulse upwards for short time periods (10 to 30 mins), increasing to between -7,500 and -7,966 kPa, and then decreasing back to -7,999 kPa (Figure 11). Two pulses lasting 1 to 7.5 hrs were observed on April 12 between 3:10 AM and 1:00 PM, increasing to between -7,310 and -6,914 kPa and then decreasing back to -7,999 kPa. Starting April 12 at 3:10 PM, sensor 2 recorded a final pulse of water, until MP exceeded FC at 10:30 PM, likely a result of the heavy rain event that day (79.3 mm). After reaching FC, the 47 cm sensor remained above -33 kPa through the end of the sampling period (June 12). Prior smaller rain events on April 1 (13 mm) and April 4 (11.4 mm) appear to have had no effect on MP at sensor 2.

Sensor 3 (96 cm) recorded small (10 min to 1.8 hr) pulses of water starting on March 20 at 2:50 PM, with MP increasing from -7,999 kPa to a maximum of -7,606 kPa. On March

22 at 11:50 AM, the pulses become longer (20 to 26 hrs) and reach a maximum of -7,024 kPa. Beginning March 25 at 6:00 PM, MP increases above -7,999 kPa for 15 days (through April 10 at 11:50 AM), reaching a maximum of -6,460 kPa (Figure 11). Finally on April 10 at 1:00 PM, a pulse of water begins at sensor 3, resulting in MP exceeding FC on April 13 at 9:20 AM. MP then remained above FC through June 12.

Beginning on April 5 at 3:20 PM, sensor 4 at 152 cm begins to record small pulses (10 to 80 min) of water, with MP increasing from -7,999 kPa to a maximum value of -7,273 kPa (Figure 11). On April 13 at 6:00 PM, the final pulse begins, with MP exceeding FC on April 14 at 3:20 AM. The MP in this zone also remains above FC until the end of the monitoring period (June 12). Thus, it appears the 79.3 mm of rain on April 12, which influenced the 47 cm and 96 cm sensors, also pushed the wetting front beyond the 152 cm sensor.

Between March 20 and April 12, the 96 cm sensor recorded a higher MP than the 47 cm sensor. During this time, matric potentials indicate water is moving downward from 12 to 47 cm, upward from 96 to 47 cm, and downward from 96 to 152 cm (Figure 11). The probable reason for higher MP at 96 cm is desiccation cracks that contribute preferential flow to this depth (e.g., Nimmo, 2010). For the 24 days that this condition persists, the sensor at 96 cm is a zero flux plane (ZFP), where upward fluid capillarity in the vadose zone is separated by downward fluid flux. The soil color changes near this depth, from a dark-colored horizon to a light-colored horizon. This change around 1 m depth (Figure 9) likely implies that the majority of macropore activity causing bioturbation from constant shrinking and swelling of smectite clays occurs in this upper portion of the soil. A typical Pedon in the Ness clay is characterized by an A horizon extending from the surface to 10 cm, a B horizon from 10 to 94 cm, and a C horizon below 94 cm (USDA Natural Resources Conservation Service, 2018).

Additional evidence for preferential flow to around 96 cm includes high gravimetric water contents in cores (0.14 to 0.21) and low chloride concentrations (15.7 to 34.5 mg L^{-1}). Water that is below the ZFP and outside of the influence of evapotranspiration, will likely become recharge water. After April 12, the MP at 47 cm increases above the MP at 96 cm, the zero flux plane no longer exists at the 96 cm depth, and fluid flux is downward to at least 152 cm (and likely deeper).

In summary, on April 12, a 79.3 mm precipitation event resulted in inundation of the playa the following day. Prior to this, the 12 cm sensor had already exceeded FC (March 29); but MP was not measured above FC in deeper intervals until April 12 (47 cm), April 13 (96 cm), and April 14 (152 cm) (Figure 11). The playa remained inundated through May 16, but all soil depths remained above FC through the end of the monitoring period (June 12). This suggests that gravity drainage is controlled by playa inundation, although downward water flux was occurring to a smaller degree in the 24 days prior to playa inundation, as evidence by the ZFP through capillarity.

A fluid flux can be calculated based on the gravity drainage wetting front, which represents fluxes for time periods during playa inundation. The gravity drainage wetting front took 14.5 days to advance from 12 to 47 cm, 10.8 hrs to move from 47 to 96 cm, and 18 hours to travel from 96 to 152 cm. From this, the calculated inundation fluid flux rate ranges from 8,800 to 400,000 mm yr^{-1} (Table A- 8). This equates to a travel time of 10 days to 1.3 yrs through the 11.5 m vadose zone. It is possible that these fast fluid fluxes equate to movement through the soil during the beginning of inundation events and rates may decrease as the soil wets and inundation persists.

Infiltrometer

K_{sat} values for playa floor and interplaya are very similar and are representative of a silt texture, which are typically between $1x10^{-6}$ to $1x10^{-4}$ cm sec^{-1} (Hillel, 2004). Values in the playa center ranged from $1.6x10^{-4} \pm 1.9x10^{-5}$ cm sec^{-1} to $7.8x10^{-4} \pm 1.5x10^{-4}$ cm sec^{-1} (Inf 1 and 2), and in the interplaya from $2.3x10^{-4} \pm 2.6x10^{-4}$ cm sec^{-1} to $7.2x10^{-4} \pm 6.8x10^{-5}$ cm sec^{-1} (Inf 3 and 4) (Figure 3 and Table A- 7). This is consistent with USDA Web Soil Survey information, which report Ulysses silt loam in the interplaya to 79 in. (201 cm), and hydric Ness clay followed by silt loam in the playa to 31 in. (79 cm) and 60 in. (152 cm), respectively (United States Department of Agriculture, 2017).

As the K_{sat} measurement is the same in the playa and interplaya location, fluid movement rates through saturated soil is the same, in the absence of macropores (in the playa). After a large rain event, soil in the interplaya may become saturated creating quick percolation, as it is in the playa. Although, it is unlikely that saturated conditions exist for long periods of time in the interplaya, as they do in the playa, due to the absence of ponding. Additionally, macropores are known to exist in the hydric soils of the playa floor, which are not present in the interplaya location, pointing to higher infiltration and fluid flux in the playa when soils are dry or partially saturated. Interplaya recharge occurs mostly during large rain events when the soil is saturated, whereas playa recharge occurs through macropores when dry or partially saturated, during large rain events when the soil is saturated, and during inundation.

Hydrus-1D Model

Results from the model indicate downward water movement in the upper soil during spring rain, but do not suggest recharge reaching the water table during the 169 days (December 26 to June 12, 2017) of the model run. The 39 cm node exceeds FC on day 94

(March 29), which is the same day that the shallow MP sensor (12 cm) reported above FC (Figure A- 7). The shallow model node (39 cm) fluid flux reaches a maximum (9,600 mm yr^{-1}) around day 110 (April 14), shortly after the large rain event on April 12 that resulted in inundation (Table A- 9). The 160 cm node exceeded FC on day 141 (May 15) and reaches a maximum of 470 mm yr^{-1} on day 152 (May 26). Deeper nodes at 510 cm and the water table (1,150 cm) remain at very low matric potentials (-8,000 kPa) and low fluxes ($2.9x10^{-6}$ mm yr^{-1}) through the entirety of the model run. By day 169 (June 12), fluid fluxes at shallow nodes (39 and 160 cm) had decreased to between 340 and 370 mm yr^{-1}. Although the modeled shallow node (39 cm) wetting aligns well with the MP measurements, the deeper nodes have delayed (160 cm) or no fluid travel (510 and 1150 cm) (Figure A- 7). This discrepancy could be due to the lack of macropores in the model calculation, and/ or the short time timeframe of the model run (169 days). Although the model did not anticipate recharge in the 169 days, the anion profiles suggest flushing to 5 and/or 9 m after playa ponding. Fluid fluxes estimated by the model suggest rapid travel times (<50 yr to 11.5 m) through the playa in the upper profile after the large rain event on April 12, and slow travel times (>10,000 yrs to 11.5 m) at deeper nodes. The maximum fluid flux in the model is within the range estimated from MP measurements during inundation (8,800 to 400,000 mm yr^{-1}). The model does support the theory that the majority of percolation beneath the playa occurs during large rain events and during inundation.

Conclusion

The Ehmke Playa study in Lane County, Kansas utilizes vadose zone anion concentrations, MP measurements, groundwater concentrations, and infiltrometer measurements to quantify recharge rates and travel times through the playa and interplaya to the HPA. Anion concentrations

in the interplaya vadose zone are overall much higher than beneath the playa, with interplaya concentrations peaking at 2 m, and then slowly decreasing to the water table. This indicates lower fluid flux rates and longer travel times through the vadose zone beneath the interplaya, compared to beneath the playa. The lower concentrations beneath the playa indicate recent flushing and mobilization of salts downwards. Lower playa vadose zone anion concentrations in pore water from 2017 (EPC 5) compared with 2016 (EPC 1 and 2) soil cores suggest the inundation event from April 13 to May 16, 2017 flushed anions from the root zone. EPC 5 exhibits a peak chloride concentration at 9 m, which is deeper than the maximum in EPC 1 (2 m) and suggests flushing of anions to 9 m during inundation. This is evidence that playa ponding events cause recharge to 9 m.

CMB calculations for the interplaya show much lower fluid fluxes and longer vadose zone travel times than the playa. Interplaya fluid fluxes range from 0.1 to 10 mm yr^{-1} with travel times between 4,800 to 5,500 yrs through the 16.7 m vadose zone. Through the playa, fluid fluxes were calculated faster (1700 mm yr^{-1}) during/ shortly after inundation events than during dry periods (78 to 118 mm yr^{-1}). This equates to a playa travel time of 8 yrs during hydroperiods and from 100 to 150 yrs between hydroperiods to the 11.5 m water table. This indicates that recharge fluid fluxes are at least one order of magnitude faster in the playa than the interplaya. These fluid fluxes and travel times are comparable to estimates from playa and interplaya regions in the SHP (Wood and Sanford, 1995; Scanlon and Goldsmith, 1997; Wood et al., 1997). Chloride concentrations measured in CHP irrigated cropland are slightly elevated when compared to concentrations measured during this study beneath the playa, but much lower than beneath the interplaya.

MP measurements indicate macropore flow, a period with a ZFP, and inundation percolation. During the 24 days prior to inundation, MP was greater at 96 cm than 47 cm, creating

a ZFP at 96 cm. Near this depth (~1 m), a higher gravimetric water content, low chloride concentration, and visible change in soil profile were observed. Combined, these findings suggest macropores facilitate water movement to this depth, with water moving away from (both upward and downward) this plane. Often, water percolating below a ZFP (~1 m) is assumed to become recharge, but anion profiles at the Ehmke Playa site suggest that transpiration is occurring deeper in the profile (~2 m). After inundation of the playa (April 12), a gravity drainage wetting front penetrated deeper intervals (47, 96, and 152 cm). During inundation (April 13 to May 16) and beyond (June 12), MP sensors report saturation and downward flux. Based on the movement of the wetting front between MP sensors, an inundation percolation rate of 8,800 to 400,000 mm yr^{-1} was calculated for the upper portion of the subsurface, which coincides to a travel time of 10 days to 1.3 yrs to the water table. This travel time is significantly faster than calculated by the CMB method, but may represent the fluid flux at the beginning of inundation events when the playa is filled with water to the annulus. The Hydrus-1D model predicted a maximum fluid flux through 39 cm of 9,600 mm yr^{-1} during spring rain, which is near the minimum calculation from the MP. By the last day of the model (day 169, June 12), the flux through 169 cm had decreased to between 340 and 370 mm yr^{-1}. This fast prediction from the model supports the MP measurements and qualifies the idea of fast percolation through the playa during rain events, but does not support fluid flux to 5 m or deeper during the 169 days modeled.

Shallow soil K_{sat} measurements indicate similar saturated soil infiltration rates in the playa and interplaya and are indicative of a silty loam. Fluid flux through the interplaya is assumed to occur only during rain events, which are sporadic, mostly in spring, and likely contribute small pulses of water downward. As the interplaya is part of the watershed, it is assumed that once the soil is saturated, the remaining water becomes overland flow and run-off to the playa. Recharge

through playa floors can occur through micropores and macropores during partial saturation, and periods of inundation. Because the interplaya is not likely saturated for extended periods, the fluid flux rate (50,000 to 240,000 mm yr^{-1}) calculated based on K_{sat} is representative of water infiltration and percolation through the playa during saturation. These data suggest a travel time of 17 to 82 days to the water table beneath the playa (11.5 m); however, saturated conditions may not persist this long as the 2017 inundation event lasted for 34 days. This inundation timeframe is less than the maximum calculated travel time, resulting in incomplete flushing. The maximum chloride concentrations in EPC 5 at 9 m suggest flushing occurred only to this depth during the 2017 inundation event and did not completely reach the water table.

Combined, the data collected at the study site indicate the playa is an area of increased recharge compared with the interplaya. While playa fluid flux can occur anytime there is a rain event, deep percolation is controlled by playa inundation. Playa ponding or inundation occurs when rain events are large enough to exceed the infiltration rate (K_{sat}) of the soil, creating excess water on the surface, which happens every 2 to 3 years. Assuming the vadose zone chloride flushing depth to 9 m (EPC 5) is representative of an inundation event every 2 to 3 years, then travel time to the water table is <10 yrs. These short travel times suggest playas provide relatively fast pathways for water and chemicals to the water table, and should be protected from contamination and degradation in order to provide recharge and maintain or improve the health of the HPA.

It appears that playas are indeed point sources of recharge to the HPA. High rates of recharge (<50 yrs) are directly related to macropores in the upper 1 m and inundation events caused by large precipitation and runoff from the surrounding watershed. Playas can also transport contaminants with flushing events, leading to compromised quality of the aquifer. Therefore, the

need to protect these areas from anthropogenic modification, sedimentation, and contaminants is important for the health of playas and their contribution to the HPA.

Future Work

Future work could continue to improve understanding of playa recharge. Pore water analysis of chlorine-36 activity would provide insight to the age of vadose zone pore water and percolation rates. Groundwater samples from the water table, in combination with pore water anion measurements and water level measurements, would provide a fluid flux estimate for comparison to other methods. Confidence in fluid flux estimates from Equation 5 could be improved by more specific quantification of run-off from the surrounding watershed. This could include gauging at the inflow or conducting an elevation analysis of the watershed to determine areas more susceptible to surface flow. The concentration of runoff water could also be measured to determine if the assumption that the chloride concentration in runoff water is the same as chloride concentration in precipitation water. MP measurements could be compared to water content reflectometers at the same depth to ensure that low MP readings near -9 kPa are indeed at saturation.

Acknowledgements

I would like to express gratitude to the US EPA in providing funding for this investigation and to the Kansas Geological Survey for conducting field work. Thank you to the University of Kansas for providing an environment for me to learn and grow into a scientist. I would like to express appreciation for my professors Randy Stotler, Bill Johnson and Dan Hirmas for supporting this project and Dakota Burt for his time completing field work and grain-size analysis. Thank you to Vance and Louise Ehmke for their interest and support in this hydrologic investigation on their property. I would like to thank my parents for supporting me and fueling my curiosity for science.

Finally, I couldn't have completed this project without the loving support from my partner, David, and my friends. Thank you.

References

Allison, G.B., and C.J. Barnes. 1985. Estimation of evaporation from the normally "dry" Lake Frome in South Australia. J. Hydrol. 78(3–4): 229–242. doi:10.1016/0022-1694(85)90103-9

Allison, G.B., and M.W. Hughes. 1978. The use of environmental chloride and tritium to estimate total recharge to an unconfined aquifer. Australia J. Soil Res. 16(2): 181-195. doi:10.1071/SR9780181

Bowen, M.W. 2011. Spatial distribution and geomorphic evolution of playa-lunette systems on the central High Plains of Kansas. Proquest LLC.: PhD Dissertation. 86 pages. https://search-proquest-com.www2.lib.ku.edu/docview/873786471?pq-origsite=primo (accessed 29 April 2018).

Bowen, M.W., and W.C. Johnson. 2012. Late quaternary environmental reconstructions of playa-lunette system evolution on the central High Plains of Kansas, United States. Bull. Geol. Soc. Am. 124(1–2): 146–161. doi:10.1130/B30382.1

Bowen, M.W., W.C. Johnson, and D.A. King. 2018. Spatial distribution and geomorphology of lunette dunes on the High Plains of Western Kansas: implications for geoarchaeological and paleoenvironmental research. Physical Geog. 39(1): 21-37. doi:10.1080/02723646.2017.1319683

Buchanan, R.C., B.B. Wilson, R.R. Buddemeier, and J.J. Butler Jr. 2015. The High Plains Aquifer. Kansas Geological Survey. Public Information Circular 18. http://www.kgs.ku.edu/Publications/pic18/index.html (accessed 29 April 2018).

Corley, J. 2003. Best Practices for establishing detection and quantification limits for pesticide residues in foods. Handbook of Residue Analytical Methods for Acrochemicals. John Wiley

& Sons Ltd. 409(c): 1-18.

Davis, S.N., D.O. Whittemore, and J. Fabryka-Martin. 1998. Uses of chloride/bromide ratios in studies of potable water. Ground Water 36(2): 338–350. doi:10.1111/j.1745-6584.1998.tb01099.x

Favre, F., P. Boivin, and M.C.S. Wopereis. 1997. Water movement and soil swelling in a dry, cracked vertisol. Geoderma 78(1–2): 113–123. doi:10.1016/S0016-7061(97)00030-X

Devlin, J.F., and P.C. Schillig. 2017. HydrogeoEstimatorXL: an Excel-based tool for estimating hydraulic gradient magnitude and direction. Hydrogeol. J. 25(3): 867-875. doi:10.1007/s10040-016-1518-4

Favre, F., P. Boivin, and M.C.S. Wopereis. 1997. Water movement and soil swelling in a dry, cracked vertisol. Geoderma 78(1–2): 113–123. doi:10.1016/S0016-7061(97)00030-X

Flint, A.L., L.E. Flint, E.M. Kwicklis, J.T. Fabryka-martin, and G.S. Bodvarsson. 2002. Estimating recharge at Yucca Mountain, Nevada, USA: comparison of methods. Hydrogeol. J. 10: 180–204. doi:10.1007/s10040-01-0169-1

Ganesan, G., K. Rainwater, D. Gitz, N. Hall, R. Zartman, W. Hudnall, and L. Smith. 2016. Comparison of infiltration flux in playa lakes in grassland and cropland basins, Southern High Plains of Texas. Texas Water J. 7(1): 25-39. https://journals.tdl.org/twj/index.php/twj/article/view/7007/pdf_12 (accessed 29 April 2018).

Gurdak, J.J., R.T. Hanson, P.B. McMahon, B.W. Bruce, J.E. McCray, G.D. Thyne, and R.C. Reedy. 2007. Climate variability controls on unsaturated water and chemical movement,

High Plains aquifer, USA. Vadose Zo. J. 6(3): 533–547. doi:10.2136/vzj2006.0087

Gurdak, J.J., and C.D. Roe. 2009. Recharge Rates and Chemistry Beneath Playas of the High Plains Aquifer - A Literature Review and Synthesis: U.S. Geological Survey Circular 1333. http://pubs.usgs.gov/circ/1333/pdf/C1333.pdf (accessed 29 April 2018).

Gurdak, J.J., M. a. Walvoord, and P.B. McMahon. 2008. Susceptibility to enhanced chemical migration from depression-focused preferential flow, High Plains aquifer. Vadose Zo. J. 7(4): 1218-1330. doi:10.2136/vzj2007.0145

Gutentag, E.D., F.J. Heimes, N.C. Krothe, R.R. Luckey, and J.B. Weeks. 1984. Geohydrology of the High Plains aquifer in parts of Colorado, Kansas, Nebraska, New Mexico, Oklahoma, South Dakota, Texas, and Wyoming. U.S. Geological Survey Prof. Pap. 1400–B. https://pubs.usgs.gov/pp/1400b/report.pdf (accessed 29 April 2018).

Herbell, M.J., and R.F. Spalding. 1993. Vadose zone fertilizer-derived nitrate and $\delta^{15}N$ extracts. Ground Water 31(3): 376–382. doi:10.1111/j.1745-6584.1993.tb01838.x

Herczeg, A.L., and M.W. Edmunds. 2000. Inorganic Ions as Tracers. p. 30–70. *In* CSIRO Land and Water, Glen Osmond, A. (ed.), Environ. Tracers in Subsurface Hydrol. Kluwer Academic Publishers.

High Plains Regional Climate Center, CLIMOD. 2018. http://climod.unl.edu/ (accessed 29 April 2018).

Hillel, D. 2004. Introduction to Environmental Soil Physics. Elsevier Science (USA), San Diego, CA.

Johnson, L.A., D.A. Haukos, L.M. Smith, and S.T. McMurry. 2012. Physical loss and

modification of Southern Great Plains playas. J. Environ. Manage. 112: 275–283. doi:10.1016/j.jenvman.2012.07.014

Kansas Data Access & Support Center. 2013. kansasgis.org/catalog (accessed 29 April 2018).

Katz, B.S., R.L. Stotler, D. Hirmas, G. Ludvigson, J.J. Smith, and D.O. Whittemore. 2016. Geochemical recharge estimation and the effects of a declining water table. Vadose Zo. J. 15(10). doi:10.2136/vzj2016.04.0031

Lindau, C.W., and R.F. Spalding. 1984. Major procedural discrepancies in soil extracted nitrate levels and nitrogen isotopic values. Ground Water 22(3): 273–278. doi:10.1111/j.1745-6584.1984.tb01399.x

Ludvigson, G.A., R.S. Sawin, E.K. Franseen, W.L. Watney, R.R. West, and J.J. Smith. 2009. A Review of the Stratigraphy of the Ogallala Formation and Revision of Neogene ("Tertiary") Nomenclature in Kansas. Kansas Current Research in Earth Sciences, Bulletin 256 Part 2. http://www.kgs.ku.edu/Current/2009/Ludvigson/Bull256part2.pdf (accessed 29 April 2018).

Maupin, M. a, and N.L. Barber. 2005. Estimated withdrawals from principal aquifers in the United States, 2000. U.S. Geological Survey Circular 1279. https://pubs.usgs.gov/circ/2005/1279/pdf/circ1279.pdf (accessed 29 April 2018).

McGuire, V.L. 2009. Water-Level Changes in the High Plains Aquifer, Predevelopment to 2007, 2005-06, and 2006-07. U.S. Geological Survey Ground-Water Resources Program, Sci. Investig. Rep. 2009-5019. https://pubs.usgs.gov/sir/2009/5019/pdf/sir2009-5019.pdf (accessed 29 April 2018)

McMahon, P.B., K.F. Dennehy, B.W. Bruce, J.K. Böhlke, R.L. Michel, J.J. Gurdak, and D.B.

Hurlbut. 2006. Storage and transit time of chemicals in thick unsaturated zones under rangeland and irrigated cropland, High Plains, United States. Water Resour. Res. 42(3). doi:10.1029/2005WR004417

Meixner, T., A.H. Manning, D.A. Stonestrom, D.M. Allen, H. Ajami, K.W. Blasch, A.E. Brookfield, C.L. Castro, J.F. Clark, D.J. Gochis, A.L. Flint, K.L. Neff, R. Niraula, M. Rodell, B.R. Scanlon, K. Singha, and M.A. Walvoord. 2016. Implications of projected climate change for groundwater recharge in the western United States. J. Hydrol. 534. doi:10.1016/j.jhydrol.2015.12.027

Nativ, R. , and R. Riggio. 1990. Precipitation in the Southern High Plains: meteorologic and isotopic features. J. of Geophysical Res. 95(D13): 22,559-22,564. doi:10.1029/JD095iD13p22559

Nimmo, J.R. 2010. Theory for Source-Responsive and Free-Surface Film Modeling of Unsaturated Flow. Vadose Zo. J. 9(2): 295-306. doi: 10.2136/vzj2009.0085

Scanlon, B.R. 1991. Evaluation of moisture flux from chloride data in desert soils. J. Hydrol. 128(1–4): 137–156. doi:10.1016/0022-1694(91)90135-5

Scanlon, B.R. 1999. Reply. Water Resour. Res. 35(2): 603–604. doi:10.1029/1998WR900073

Scanlon, B.R., C.C. Faunt, L. Longuevergne, R.C. Reedy, W.M. Alley, V.L. McGuire, and P.B. McMahon. 2012. Groundwater depletion and sustainability of irrigation in the US High Plains and Central Valley. Proc. Natl. Acad. Sci. 109(24): 9320–9325. doi:10.1073/pnas.1200311109

Scanlon, B.R., and R.S. Goldsmith. 1997. Field study of spatial variability in unsaturated flow

beneath and adjacent to playas. Water Resour. Res. 33(10): 2239-2252. doi:10.1029/97WR01332

Scanlon, B.R., R.C. Reedy, D.A. Stonestrom, D.E. Prudic, and K.F. Dennehy. 2005. Impact of land use and land cover change on groundwater recharge and quality in the southwestern US. Glob. Chang. Biol. 11(10): 1577–1593. doi:10.1111/j.1365-2486.2005.01026.x

Scanlon, B.R., D.A. Stonestrom, R.C. Reedy, F.W. Leaney, J. Gates, and R.G. Cresswell. 2009. Inventories and mobilization of unsaturated zone sulfate, fluoride, and chloride related to land use change in semiarid regions, southwestern United States and Australia. Water Resour. Res. 45(7). doi:10.1029/2008WR006963

Simunek, J., M. Sejna, H. Saito, M. Sakai, and M.Th. van Genuchten. 2009. The HYDRUS-1D software package for simulating the one-dimensional movement of water, heat, and multiple solutes in variably-saturated media. Dep. of Environ. Sci., Univ. of Calif., Riverside. Version 4.08. https://www.pc-progress.com/Downloads/Pgm_hydrus1D/HYDRUS1D-4.08.pdf (accessed 29 April 2018).

Stonestrom, D.A., D.E. Prudic, R.J. Laczniak, K.C. Akstin, R.A. Boyd, and K.K. Henlelman. 2003. Estimates of Deep percolation Beneath Native Vegetation, Irrigated Fields, and the Amargosa-River Channel, Amargosa Desert, Nye County, Nevada. USGS Open File Rep. 03-104: 83. https://pubs.usgs.gov/of/2003/ofr03-104/pdf/OFR-03-104_ver1.02.pdf (accessed 29 April 2018).

United States Dept of Agriculture. Natural Resource Conservation Service. Official Soil Series Descriptions and Series Classification. https://soilseries.sc.egov.usda.gov/ (accessed 29 April 2018).

United States Department of Agriculture, N.R.C.S. 2017. Web Soil Survey. https://websoilsurvey.sc.egov.usda.gov (accessed 29 April 2018).

Water Information Management and Analysis System, ver 5. 2018. Kansas Geological Survey. University of Kansas, Lawrence. http://hercules.kgs.ku.edu/geohydro/wimas/query_setup.cfm?CFID=10418598&CFTOKEN=59269962&jsessionid=5a30126580006d6c56d5 (accessed 29 April 2018).

Whittemore, D.O. 1993. Ground-water geochemistry in the mineral intrusion area of Groundwater Management District no. 5, south-central Kansas. Kansas Geological Survey Open-File Report 93-2. http://www.kgs.ku.edu/Hydro/Publications/1993/OFR93_2/OFR93-2.pdf (accessed 29 April 2018).

Whittemore, D.O. 1995. Geochemical differentiation of oil and gas brine from other saltwalter sources contaminating water resources: Case studies from Kansas and Oklahoma. Environ. Geosci. 2(1): 15–31. ISSN: 1075-9565.

Wilson, R.D. 2010. Evaluating hydroperiod response in the Rainwater Basin wetlands of south-central Nebraska. University of Nebraska-Lincoln. Master's Thesis. https://digitalcommons.unl.edu/cgi/viewcontent.cgi?article=1009&context=natresdiss (accessed 29 April 2018)

Wood, W.W. 1997. Comment on “Field study of spatial variability in unsaturated flow beneath and adhacent to playas.” Water Resour. Res. 33(2): 2239–2252. doi:10.1029/1998WR900072

Wood, W.W., K.A. Rainwater, and D.B. Thompson. 1997. Quantifying macropore recharge: Examples from a semi-arid area. Ground Water 35(6): 1097–1106. doi:10.1111/j.1745-

6584.1997.tb00182.x

Wood, W.W., and W.E. Sanford. 1995. Chemical and isotopic methods for quantifying ground-water recharge in a regional, semiarid environment. Ground Water 33(3): 458–468. doi:10.1111/j.1745-6584.1995.tb00302.x

Tables

Table 1. Playa anion concentrations in pore water (mg L^{-1}) and field water contents for EPC 1, 2, and 5.

Core Sample	Average Depth (m)	Chloride (mg L^{-1})	Bromide (mg L^{-1})	Nitrate-N (mg L^{-1})	Sulfate (mg L^{-1})	Fluoride (mg L^{-1})	θG	θV
EPC 1-1	0.025	81	5.4	<0.2	450	6.9	0.13	0.14
EPC 1-1	0.775	22	4.5	<0.2	170	14	0.14	0.17
EPC 1-2	1.695	42	4.2	<0.2	220	5.3	0.08	0.09
EPC 1-2	1.995	140	<0.1	<0.2	360	14	0.05	0.06
EPC 1-3	2.575	25	3.2	<0.2	170	4.2	0.10	0.16
EPC 1-3	3.025	16	<0.1	<0.2	130	<0.2	0.15	0.17
EPC 1-3	3.325	14	1.9	<0.2	110	2.7	0.18	0.21
EPC 1-4	4.085	16	1.7	<0.2	200	10	0.19	0.19
EPC 1-4	4.685	31	1.7	<0.2	190	14	0.19	0.20
EPC 1-5	5.125	60	1.7	0.83	270	8.0	0.24	0.30
EPC 2-1	0.025	96	6.5	<0.2	370	8.8	0.12	0.14
EPC 2-1	0.765	16	3.2	<0.2	120	1.3	0.15	0.15
EPC 2-2	1.715	21	3.0	<0.2	150	16	0.12	0.16
EPC 2-2	2.015	25	<0.1	<0.2	130	12	0.12	0.18
EPC 2-3	2.615	19	2.7	<0.2	170	8.2	0.12	0.14
EPC 2-3	3.075	14	<0.1	<0.2	150	9.7	0.16	0.16
EPC 2-3	3.365	12	2.0	<0.2	190	10	0.18	0.19
EPC 2-4	4.115	15	2.0	<0.2	220	16	0.18	0.22
EPC 2-4	4.725	37	2.0	<0.2	210	11	0.18	0.18
EPC 2-5	5.185	78	1.8	<0.2	310	9.5	0.22	0.25
EPC 5-2	0.515	51	<0.1	<0.2	110	2.8	0.18	0.31
EPC 5-3	1.015	35	<0.1	<0.2	83	3.4	0.21	0.29
EPC 5-4	2.015	37	<0.1	<0.2	110	5.3	0.16	0.26
EPC 5-6	3.015	27	<0.1	<0.2	180	7.0	0.19	0.29
EPC 5-8	4.015	29	<0.1	<0.2	190	13	0.21	0.25
EPC 5-9	5.015	46	<0.1	<0.2	330	18	0.24	0.31
EPC 5-11	6.015	19	<0.1	<0.2	82	17	0.16	0.26
EPC 5-12	7.015	34	<0.1	1.5	120	29	0.23	0.34
EPC 5-14	8.015	37	<0.1	2.4	78	40	0.11	0.18
EPC 5-15	9.015	72	<0.1	3.4	120	60	0.06	0.10
EPC 5-16	10.015	63	<0.1	2.4	58	47	0.10	0.16
EPC 5-18	11.015	55	<0.1	2.1	63	27	0.19	0.33
EPC 5-19	11.685	34	<0.1	<0.2	82	17	0.21	0.28

Table 2. Interplaya anion concentrations in pore water (mg L^{-1}) and field water contents for EPC 7.

Core Sample	Average Depth (m)	Chloride (mg L^{-1})	Bromide (mg L^{-1})	Nitrate-N (mg L^{-1})	Sulfate (mg L^{-1})	Fluoride (mg L^{-1})	θG	θV
EPC 7-2	0.515	59	<0.1	<0.2	59	11	0.13	0.22
EPC 7-3	1.015	220	0.91	<0.2	1100	44	0.15	0.18
EPC 7-4	2.015	3900	18	<0.2	2600	4.0	0.13	0.17
EPC 7-6	3.015	1400	6.5	3.5	1200	15	0.13	0.17
EPC 7-8	4.015	860	5.0	4.7	850	30	0.13	0.20
EPC 7-9	5.015	640	3.0	7.6	500	48	0.16	0.20
EPC 7-11	6.015	450	2.6	7.1	380	63	0.16	0.25
EPC 7-12	7.015	340	1.5	<0.2	360	66	0.12	0.23
EPC 7-14	7.905	260	1.0	<0.2	270	43	0.11	0.21
EPC 7-15	9.015	270	1.1	<0.2	230	35	0.12	0.21
EPC 7-16	10.675	85	<0.1	<0.2	130	21	0.22	0.30
EPC 7-17	11.415	58	<0.1	<0.2	140	29	0.09	0.18
EPC 7-18	12.655	31	<0.1	<0.2	94	22	0.13	0.20
EPC 7-19	14.065	41	<0.1	<0.2	140	38	0.11	0.15
EPC 7-21	15.515	46	<0.1	<0.2	220	56	0.11	0.22
EPC 7-22	16.015	45	<0.1	<0.2	83	32	0.12	0.20
EPC 7-23	16.745	42	<0.1	<0.2	69	25	0.28	0.34

Table 3. Playa anion vadose zone ratios from pore water (mass ratio, mg L^{-1}) for EPC 1, 2, and 5. Some ratios are reported as not-applicable (NA) due to certain measurements of bromide and nitrate that are below the instrument quantification limit.

Core Sample	Average Depth (m)	Bromide/ Chloride	Nitrate/ Chloride	Sulfate/ Chloride	Fluoride/ Chloride
EPC 1-1	0.025	0.068	NA	5.6	0.085
EPC 1-1	0.775	0.20	NA	7.6	0.64
EPC 1-2	1.695	0.099	NA	5.2	0.13
EPC 1-2	1.995	NA	NA	2.7	0.10
EPC 1-3	2.575	0.13	NA	6.9	0.17
EPC 1-3	3.025	NA	NA	8.3	0
EPC 1-3	3.325	0.14	NA	8.0	0.20
EPC 1-4	4.085	0.11	NA	12	0.62
EPC 1-4	4.685	0.056	NA	6.2	0.44
EPC 1-5	5.125	0.029	0.014	4.4	0.13
EPC 2-1	0.025	0.068	NA	3.8	0.091
EPC 2-1	0.765	0.20	NA	7.8	0.084
EPC 2-2	1.715	0.14	NA	7.1	0.74
EPC 2-2	2.015	NA	NA	5.2	0.48
EPC 2-3	2.615	0.14	NA	9.3	0.44
EPC 2-3	3.075	NA	NA	10	0.67
EPC 2-3	3.365	0.16	NA	16	0.84
EPC 2-4	4.115	0.13	NA	15	1.1
EPC 2-4	4.725	0.055	NA	5.7	0.30
EPC 2-5	5.185	0.023	NA	4.0	0.12
EPC 5-2	0.515	NA	NA	2.2	0.054
EPC 5-3	1.015	NA	NA	2.4	0.099
EPC 5-4	2.015	NA	NA	2.9	0.15
EPC 5-6	3.015	NA	NA	6.8	0.26
EPC 5-8	4.015	NA	NA	6.6	0.46
EPC 5-9	5.015	NA	NA	7.1	0.38
EPC 5-11	6.015	NA	NA	4.4	0.91
EPC 5-12	7.015	NA	0.046	3.7	0.85
EPC 5-14	8.015	NA	0.064	2.1	1.1
EPC 5-15	9.015	NA	0.047	1.6	0.82
EPC 5-16	10.015	NA	0.039	0.92	0.74
EPC 5-18	11.015	NA	0.038	1.1	0.50
EPC 5-19	11.685	NA	NA	2.4	0.51

Table 4. Interplaya anion vadose zone ratios from pore water (mass ratio, mg L^{-1}) for EPC 7. Some ratios are reported as not-applicable (NA) due to certain measurements of bromide and nitrate that are below the instrument quantification limit.

Core Sample	Average Depth (m)	Bromide/ Chloride	Nitrate/ Chloride	Sulfate/ Chloride	Fluoride/ Chloride
EPC 7-2	0.515	NA	NA	0.99	0.18
EPC 7-3	1.015	0.0041	NA	4.7	0.20
EPC 7-4	2.015	0.0046	NA	0.67	0.0010
EPC 7-6	3.015	0.0046	0.0024	0.83	0.01
EPC 7-8	4.015	0.0059	0.0055	1.00	0.04
EPC 7-9	5.015	0.0047	0.012	0.78	0.07
EPC 7-11	6.015	0.0059	0.016	0.85	0.14
EPC 7-12	7.015	0.0045	NA	1.1	0.19
EPC 7-14	7.905	0.0040	NA	1.0	0.17
EPC 7-15	9.015	0.0040	NA	0.86	0.13
EPC 7-16	10.675	NA	NA	1.6	0.25
EPC 7-17	11.415	NA	NA	2.5	0.49
EPC 7-18	12.655	NA	NA	3.1	0.72
EPC 7-19	14.065	NA	NA	3.6	0.93
EPC 7-21	15.515	NA	NA	4.9	1.2
EPC 7-22	16.015	NA	NA	1.8	0.71
EPC 7-23	16.745	NA	NA	1.6	0.60

Table 5. Depth-weighted mass averages (mg L^{-1}) for vadose zone anion concentrations and water contents.

Core	Total Depth (m)	Chloride (mg L^{-1})	Bromide (mg L^{-1})	Nitrate-N (mg L^{-1})	Sulfate (mg L^{-1})	Fluoride (mg L^{-1})	θG	θV
EPC 1	5.1	35	2.5	0.33	200	8.3	0.14	0.17
EPC 2	5.2	26	2.2	0.28	180	11	0.16	0.18
EPC 5	11.7	42	<0.1	1.2	130	24	0.17	0.25
EPC 7	16.7	520	2.4	1.5	480	35	0.14	0.22

Table 6. Groundwater well surface elevations, total depths below ground surface (bgs), and measured water levels bgs.

Well Name	Land Surface Elevation (m)	Total Well Depth (m bgs)	----------Measured Water Levels (m bgs)----------			
			6/25/2016	7/28/2016	6/12/2017	8/21/2017
Well 1	867.84	31.53	11.56	11.55	11.49	11.48
Well 2	871.60	30.13	16.08	16.09	15.97	16.03
Well 3	874.16	29.98	16.45	16.50	16.43	16.44

Table 7. Groundwater anion concentrations (mg L^{-1}) collected in August, 2017.

Well Name	Chloride	Bromide	Nitrate-N	Sulfate	Fluoride
Well 1	21	<0.1	1.1	71	2.7
Well 2	24	0.14	1.5	65	2.4
Well 3	26	0.11	1.5	82	2.9
East Windmill Well	20	0.20	1.0	48	1.8

Table 8. Groundwater well anion concentration ratios (mass ratio, mg L^{-1}) collected in August, 2017. The bromide/chloride ratio in Well 1 is not-applicable (NA) due to bromide concentrations below the instrument quantification limit.

Well Name	Bromide/ Chloride	Nitrate/ Chloride	Sulfate/ Chloride	Fluoride/ Chloride
Well 1	NA	0.054	3.4	0.13
Well 2	0.0058	0.060	2.7	0.10
Well 3	0.0040	0.056	3.1	0.11
East Windmill Well	0.010	0.051	2.5	0.09

Table 9. Anion concentrations, fluid fluxes and travel times in the Southern High Plains.

Publication	Site Description	Chloride (mg L^{-1})	Sulfate (mg L^{-1})	Fluoride (mg L^{-1})	Fluid Flux (mm yr^{-1})	Travel Time to Aquifer (yrs)	Vadose Zone Thickness (m)
Wood and Sanford, 1995	Playa	17 to 111			77		
	Interplaya (dune)	39 to 19,293					
Scanlon and Goldsmith, 1997*	Playa	16 to 451			60 to 100		
	Interplaya	324 to 4171			0.1 to 4	5500 to 9900	4.5 to 17.7
Wood et al., 1997	Playa	0.3 to 55			Interstitial: 22 to 34 Total: 750 to 2720		
Scanlon et al., 2009 (averages)	Rangeland	860 to 2,300	2500 to 7700	80 to 87		17000 to 29000	8.3 to 29
	Rain-Fed Agriculture	3.7 to 740	71 to 5000	35 to 77	5 to 92		4 to 11.4
Ganesan et al., 2016 (averages)	Playa with Grassland Watershed				330 to 1700		
	Playa with Cropland Watershed				730 to 7200		

*Chloride concentration range includes mean and maximum values.

Table 10. Anion concentrations, fluid fluxes and travel times in the Northern and Central High Plains.

Publication	Site Description	Chloride	Sulfate	Bromide	Nitrate	Fluid Flux (mm yr^{-1})	Travel Time (yrs)	Vadose Zone Thickness (m)
*McMahon et al., 2006	CHP Rangeland	0 to 32			0 to 290	0.2 to 5	2,000	50
	CHP Irrigated Cropland	0 to 55			0 to 19	39 to 54	49 to 130	17 to 45
Gurdak et al., 2007 (flux is regional ave.)	CHP Rangeland (mg kg^{-1})	1 to 42			0 to 250	196 to 390		
Katz et al., 2017	NHP Irrigated Cropland (mg L^{-1})	24 to 387	0 to 1,900	0 to 2.7	0 to 450	27 to 138	45	35**
	NHP Irrigated Cropland (mg kg^{-1})	1 to 48	0 to 230	0.01 to 0.2	0 to 55			
Meixner et al., 2017	Entire CHP (regional ave.)					18		

*Unless otherwise stated, chloride reported as mg L^{-1}, nitrate reported as mg kg^{-1}

**Depth represents the predevelopment water table, actual water table is at 64 m

Table 11. Ehmke Playa site fluid flux ranges and travel times to the High Plains aquifer.

Location	Depth (m)	Depth-Wt. Fluid Flux Eq. 4 (q_1, mm yr^{-1})	Depth-Wt. Fluid Flux Eq. 5 (q_2, mm yr^{-1})			Depth-Wt. Fluid Flux Eq. 6 (q_3, mm yr^{-1})	
			R as 5% of P	R as 10% of P	R as 20% of P	2016 Core	2017 Core
EPC 1	5.1	12	28	45	78	78 to 118	NA
EPC 2	5.2	15	37	58	100	NA	NA
EPC 5	11.5	8	20	31	54	NA	1700
EPC 7	16.7	4	NA	NA	NA	NA	NA

Location	Depth (m)	Travel Times (yrs) Calculated from Eq. 7 (tt_1) with Corresponding Above Fluid Fluxes Used for q						Travel time (yrs) from Eq. 8 (tt_2)
EPC 1	5.1	430	180	110	65	100 to 150*	NA	92
EPC 2	5.2	340	140	90	52	NA	NA	84
EPC 5	11.5	1400	580	370	210	NA	8	390
EPC 7	16.7	4800	NA	NA	NA	NA	NA	5500

Figures

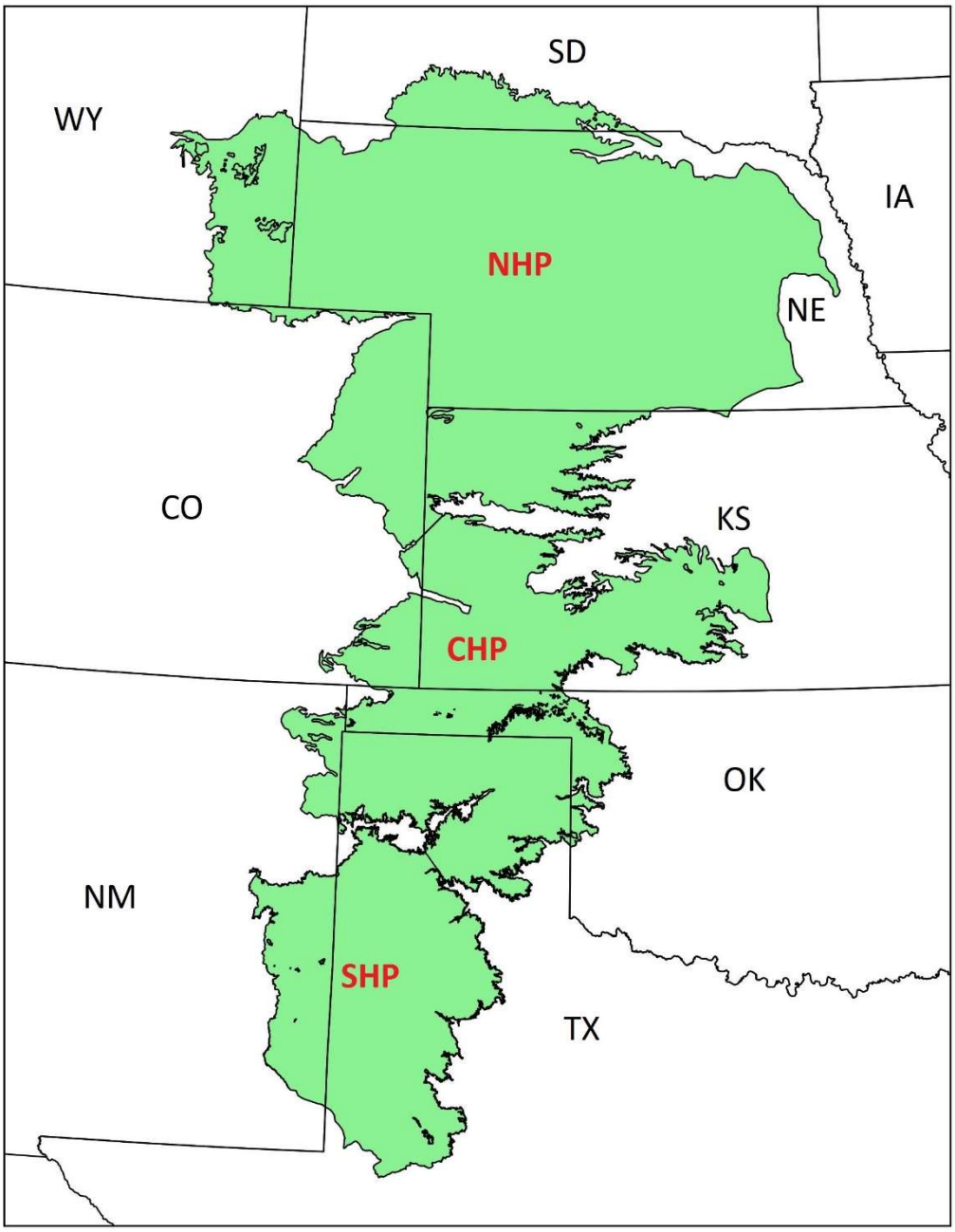

Figure 1. Aerial extent of the High Plains aquifer showing the three separate areas delineated as the Northern High Plains (NHP), Central High Plains (CHP) and Southern High Plains (SHP) (Kansas Data Access & Support Center, 2013).

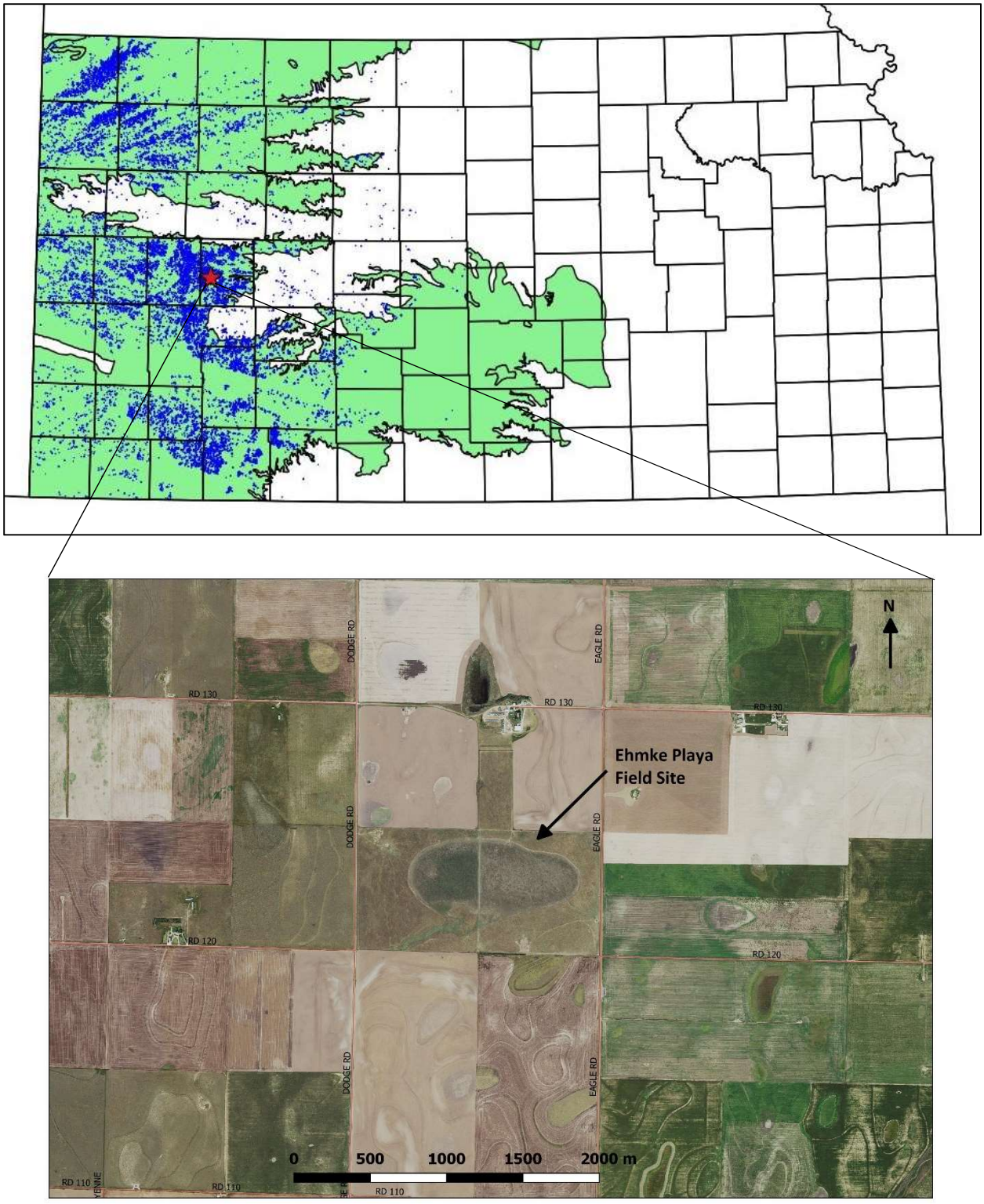

Figure 2. Western Kansas with High Plains aquifer extent shown in green, playas shown in blue, and Ehmke Playa site field location at the red star (Kansas Data Access & Support Center, 2013).

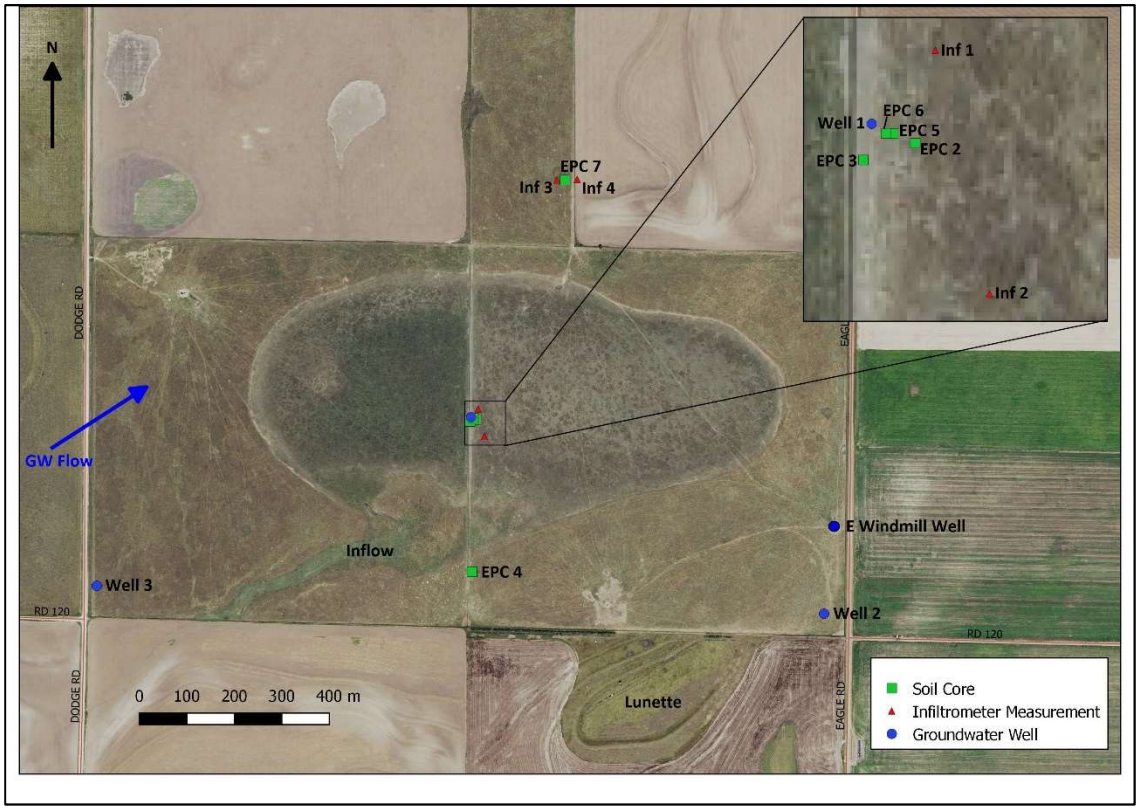

Figure 3. Ehmke Playa site with sample locations (Kansas Data Access & Support Center, 2013).

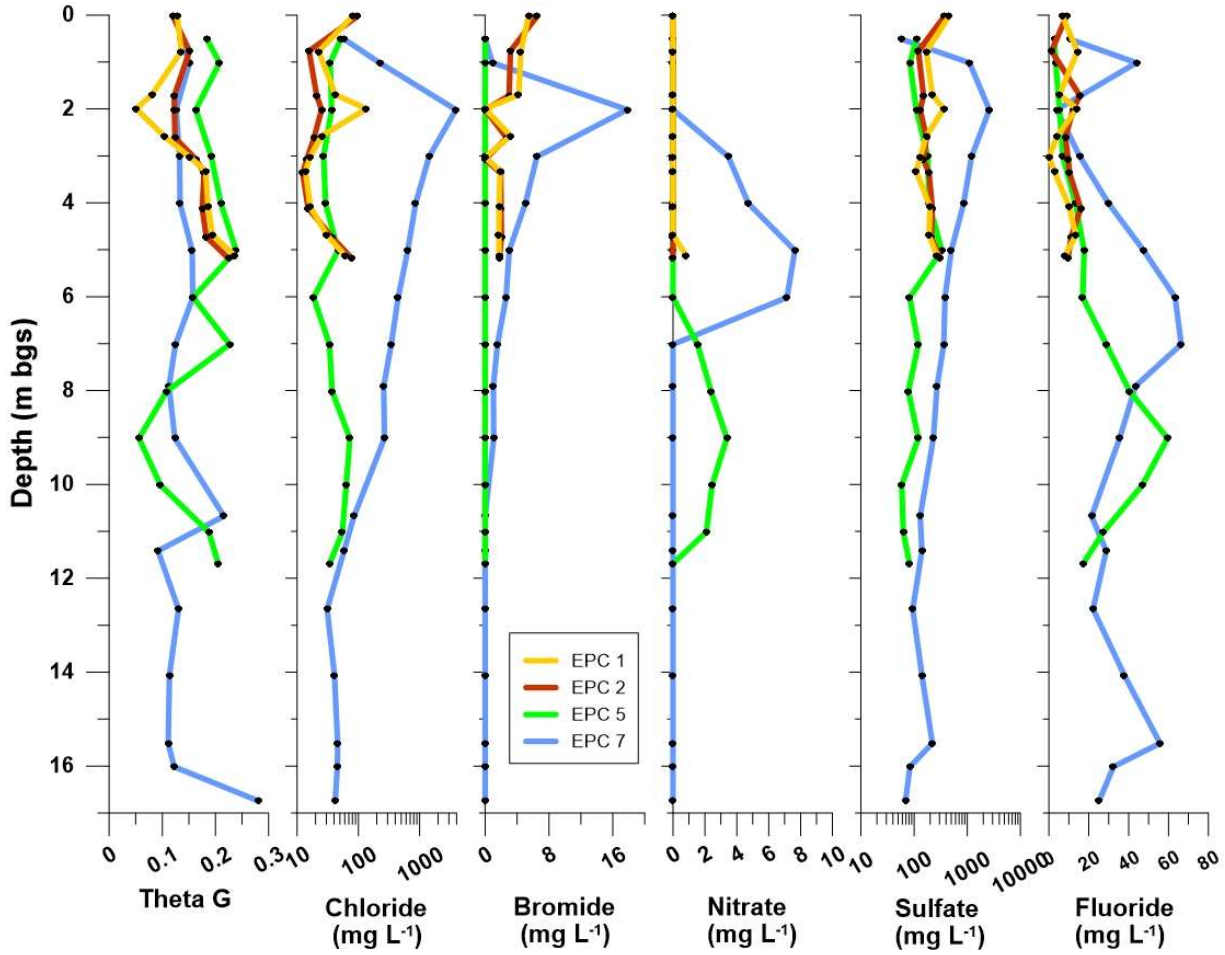

Figure 4. Gravimetric water content and anion depth profiles for playa (EPC 1, 2, 5) and interplaya (EPC 7) cores. Anion concentrations are reported as mg L^{-1} of pore water.

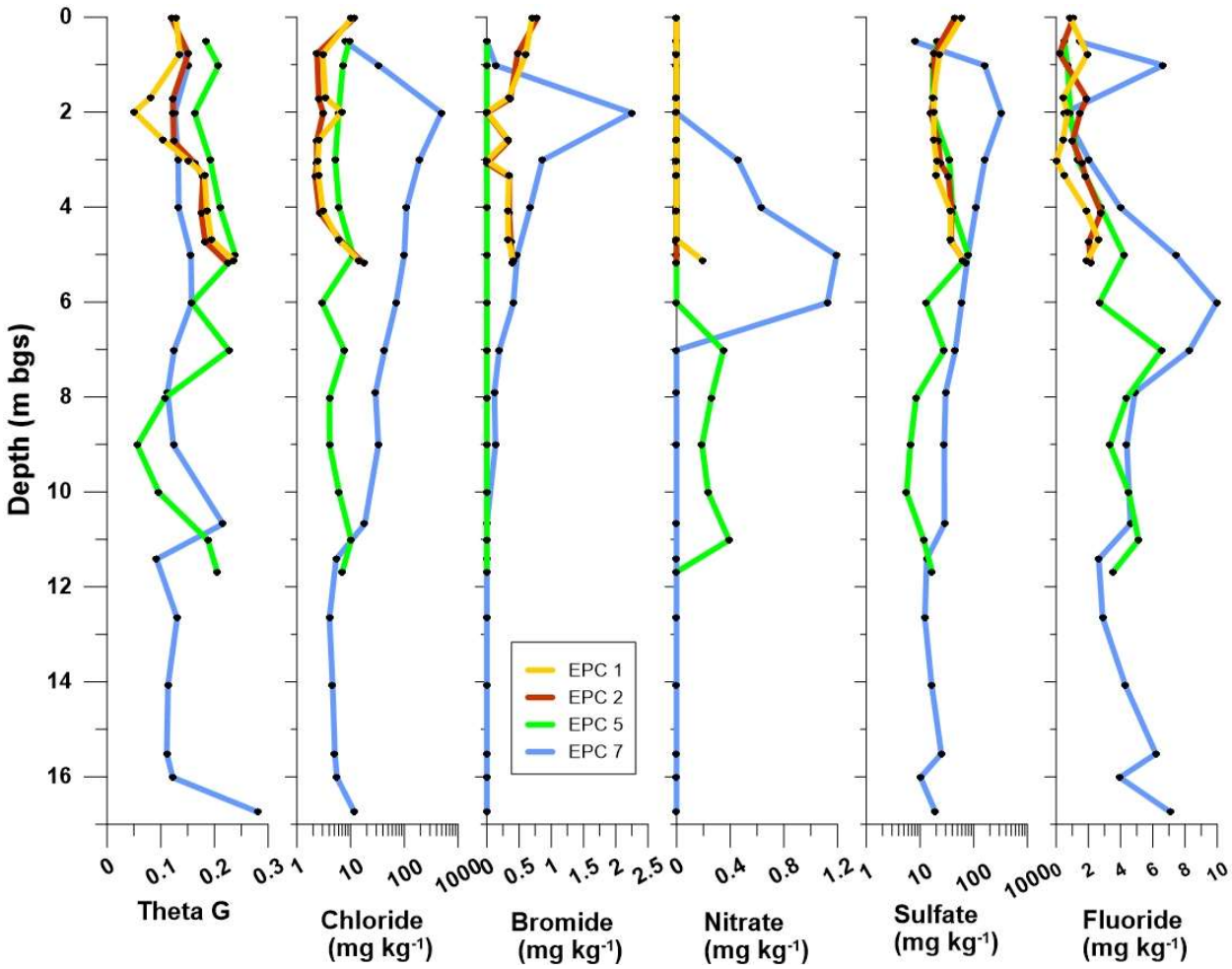

Figure 5. Gravimetric water content and anion depth profiles for playa (EPC 1, 2, 5) and interplaya (EPC 7) cores. Anion concentrations are reported as mg kg^{-1} of soil.

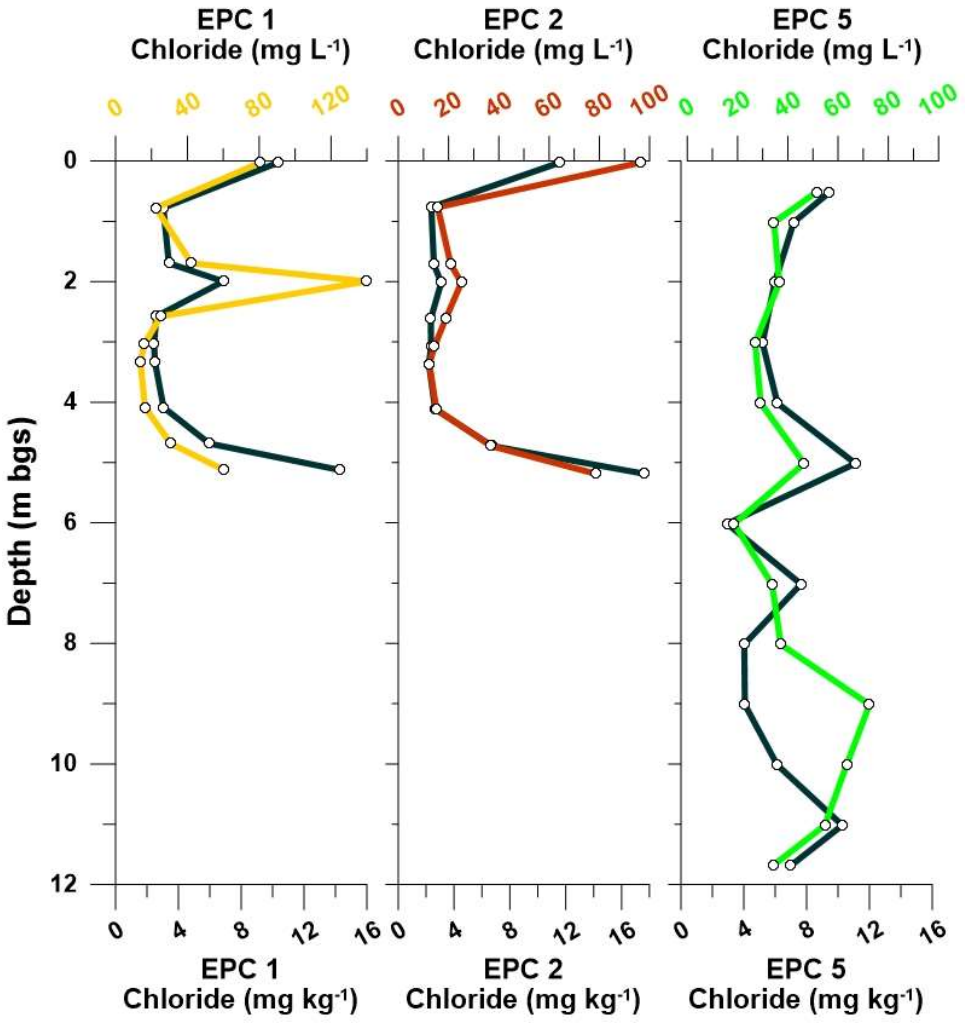

Figure 6. Playa anion depth profiles reported both as mg L^{-1} and mg kg^{-1} for 2016 (EPC 1 and 2) and 2017 (EPC 5) playa cores.

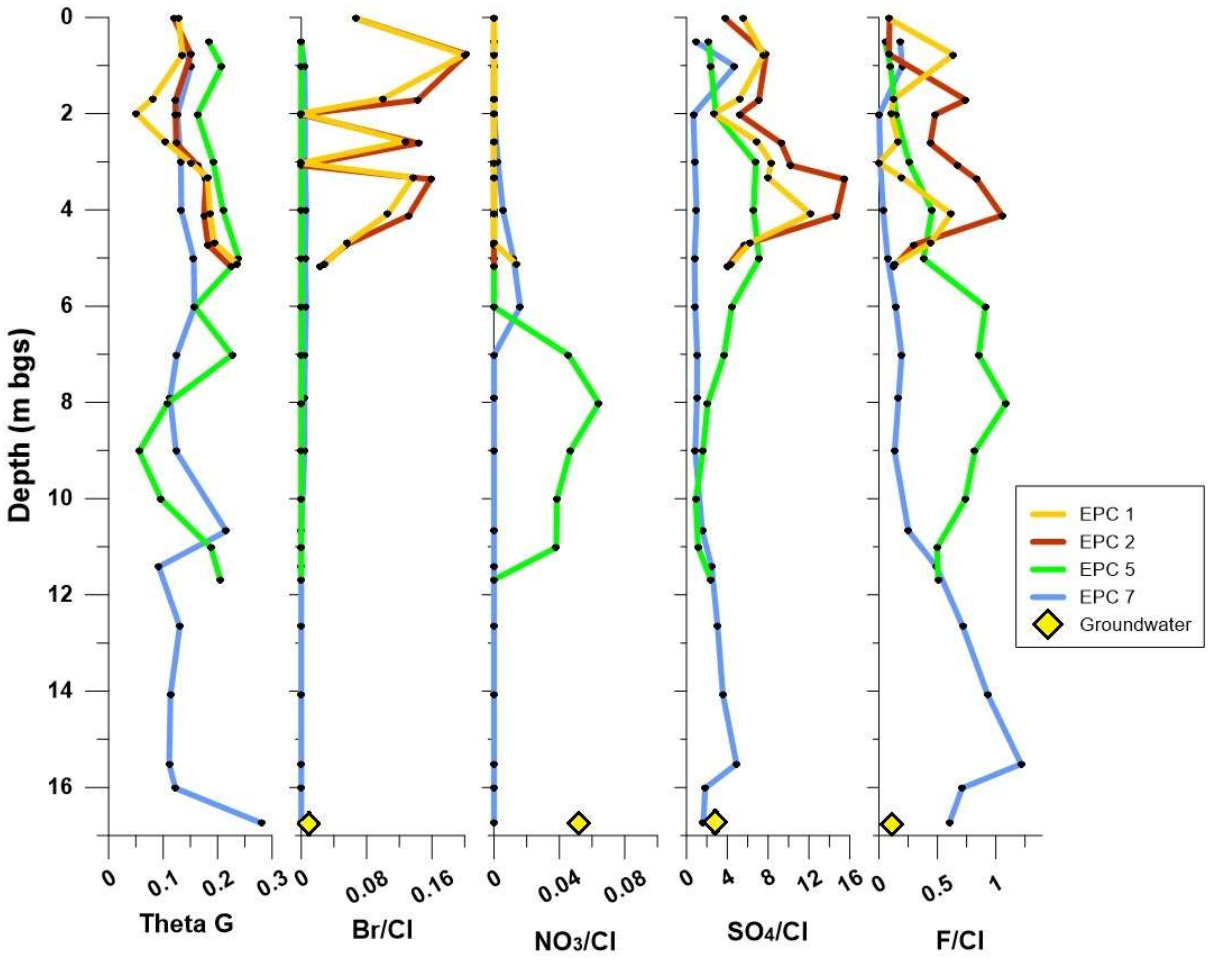

Figure 7. Vadose zone anion ratios (mass ratio, mg L^{-1}) for playa (EPC 1, 2, and 5) and interplaya (EPC 7) cores. Yellow diamonds represent groundwater concentrations in the four sampled wells. Depth location of groundwater marker does not reflect actual groundwater level.

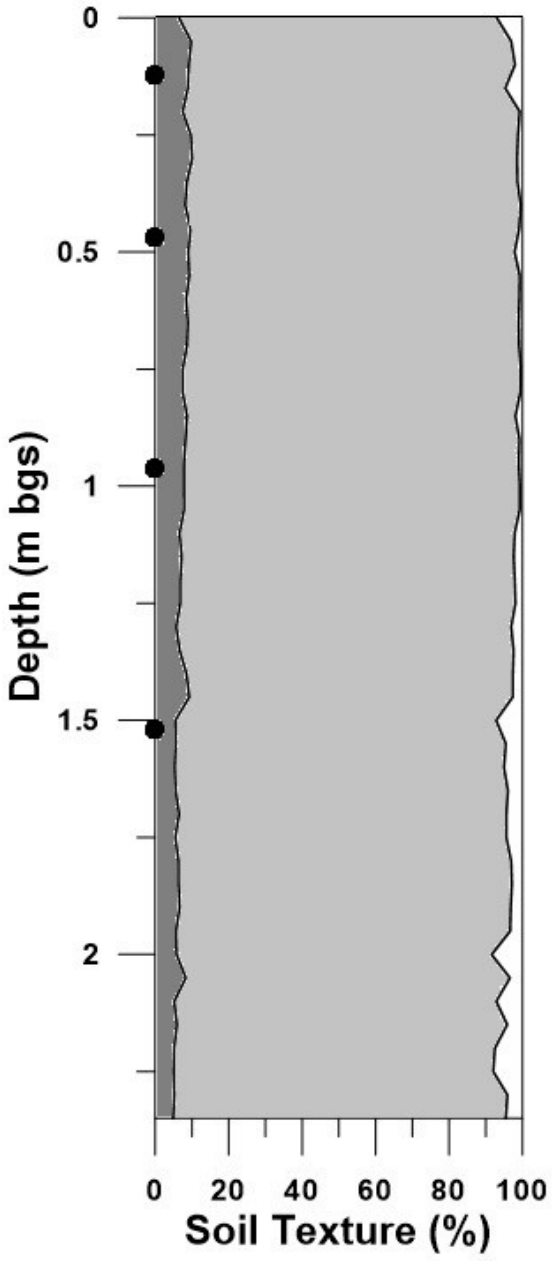

Figure 8. Soil texture of the pit in center of playa to a depth of 2.35 m below ground surface (bgs). Black dots are locations of matric potential sensors. Dark gray is clay%, light gray is silt% and white is sand%.

Figure 9. Image from excavated pit in playa center with red circles indicating depth of installed water potential sensors at 12, 47, 96, and 152 cm.

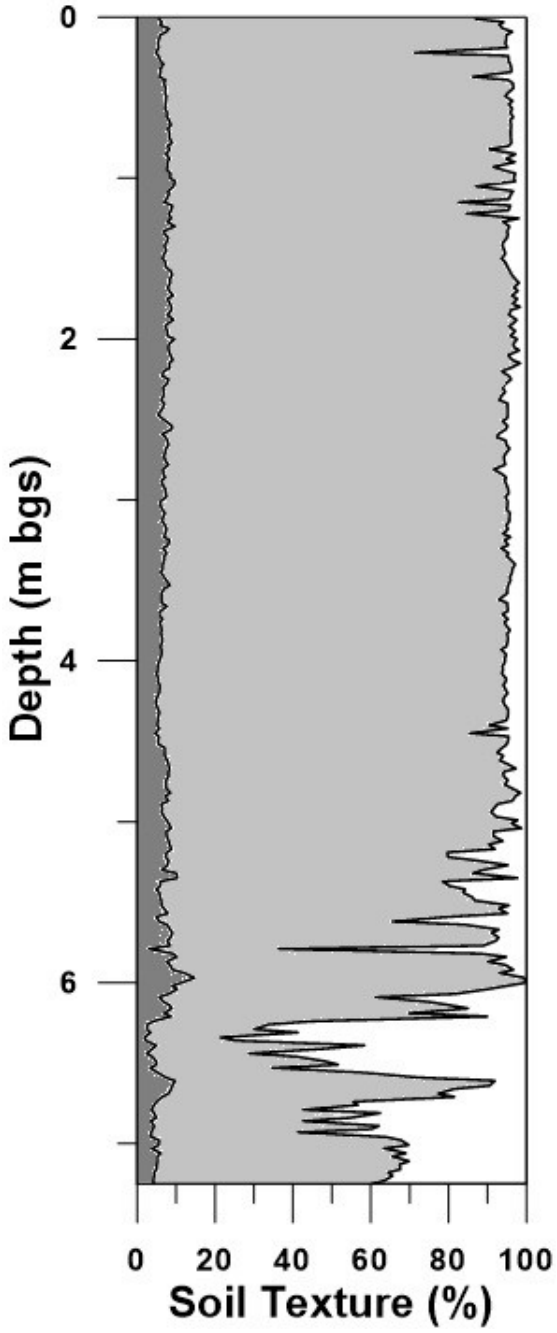

Figure 10. Texture of EPC 4 to 7.25 m below ground surface (bgs). Dark gray is clay%, light gray is silt% and white is sand%.

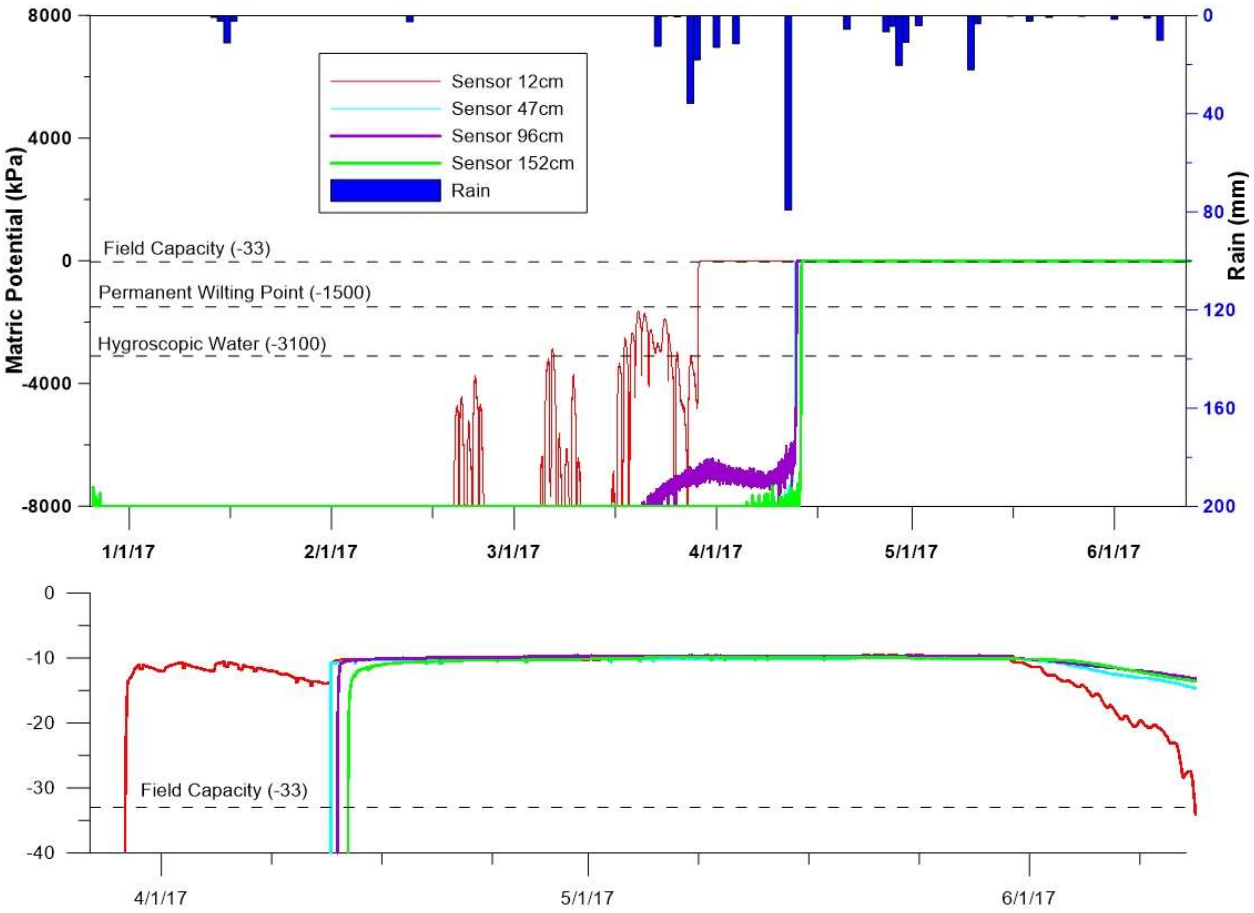

Figure 11. Upper graph: matric potential (kPa) from 12/26/16 to 6/12/17 and daily rainfall (mm). Lower graph: zoom of 3/30/17 to 6/12/17 when field capacity is exceeded and gravity drainage is underway, which corresponds to a playa inundation from April 13 to May 16.

Supplementary Tables Appendix 1

Table A- 1. GPS locations of monitoring wells, soil borings, and infiltrometer measurements.

Name	Type	Latitude	Longitude
Well 1	Groundwater Monitoring Well	38.44240	-100.60301
Well 2	Groundwater Monitoring Well	38.43879	-100.59441
Well 3	Groundwater Monitoring Well	38.43908	-100.61197
EPC 1	2016 Soil Core	38.44236	-100.60289
EPC 2	2016 Soil Core	38.44236	-100.60289
EPC 3	2016 Soil Core	38.44232	-100.60303
EPC 4	2016 Soil Core	38.43947	-100.60292
EPC 5	2017 Soil Core	38.44238	-100.60295
EPC 6	2017 Soil Core	38.44238	-100.60297
EPC 7	2017 Soil Core	38.44693	-100.60084
Inf 1	Infiltrometer Measurement	38.44256	-100.60284
Inf 2	Infiltrometer Measurement	38.44204	-100.60268
Inf 3	Infiltrometer Measurement	38.44693	-100.60104
Inf 4	Infiltrometer Measurement	38.44695	-100.60055

Table A- 2. Playa anion concentrations in bulk soil (mg kg^{-1}) for EPC 1, 2, and 5. Instrument quantification limits (IQLs) are displayed in Table A- 6.

Core Sample	Average Depth (m)	Chloride (mg kg^{-1})	Bromide (mg kg^{-1})	Nitrate-N (mg kg^{-1})	Sulfate (mg kg^{-1})	Fluoride (mg kg^{-1})
EPC 1-1	0.025	10	0.70	<IQL	58	0.88
EPC 1-1	0.775	3.0	0.61	<IQL	23	1.9
EPC 1-2	1.695	3.4	0.34	<IQL	18	0.43
EPC 1-2	1.995	6.9	<IQL	<IQL	18	0.71
EPC 1-3	2.575	2.6	0.33	<IQL	18	0.43
EPC 1-3	3.025	2.4	<IQL	<IQL	20	<IQL
EPC 1-3	3.325	2.5	0.34	<IQL	20	0.49
EPC 1-4	4.085	3.0	0.32	<IQL	37	1.9
EPC 1-4	4.685	6.0	0.33	<IQL	37	2.6
EPC 1-5	5.125	14	0.41	0.20	63	1.9
EPC 2-1	0.025	12	0.78	<IQL	44	1.1
EPC 2-1	0.765	2.4	0.48	<IQL	18	0.20
EPC 2-2	1.715	2.6	0.36	<IQL	18	1.9
EPC 2-2	2.015	3.1	<IQL	<IQL	16	1.5
EPC 2-3	2.615	2.3	0.33	<IQL	22	1.0
EPC 2-3	3.075	2.4	<IQL	<IQL	24	1.6
EPC 2-3	3.365	2.2	0.35	<IQL	34	1.8
EPC 2-4	4.115	2.6	0.35	<IQL	39	2.8
EPC 2-4	4.725	6.7	0.37	<IQL	38	2.0
EPC 2-5	5.185	18	0.40	<IQL	70	2.1
EPC 5-2	0.515	9.5	<IQL	<IQL	21	0.51
EPC 5-3	1.015	7.2	<IQL	<IQL	17	0.71
EPC 5-4	2.015	6.0	<IQL	<IQL	17	0.87
EPC 5-6	3.015	5.2	<IQL	<IQL	35	1.3
EPC 5-8	4.015	6.1	<IQL	<IQL	40	2.8
EPC 5-9	5.015	11	<IQL	<IQL	79	4.2
EPC 5-11	6.015	2.9	<IQL	<IQL	13	2.7
EPC 5-12	7.015	7.6	<IQL	0.35	28	6.5
EPC 5-14	8.015	4.0	<IQL	0.26	8.4	4.4
EPC 5-15	9.015	4.1	<IQL	0.19	6.6	3.3
EPC 5-16	10.015	6.1	<IQL	0.24	5.6	4.5
EPC 5-18	11.015	10	<IQL	0.39	12	5.1
EPC 5-19	11.685	7.0	<IQL	<IQL	17	3.5

Table A- 3. Interplaya anion concentrations in bulk soil (mg kg^{-1}) for EPC 7. Instrument quantification limits (IQLs) are displayed in Table A- 6.

Core Sample	Average Depth (m)	Chloride (mg kg^{-1})	Bromide (mg kg^{-1})	Nitrate-N (mg kg^{-1})	Sulfate (mg kg^{-1})	Fluoride (mg kg^{-1})
EPC 7-2	0.515	8.0	<IQL	<IQL	7.9	1.4
EPC 7-3	1.015	34	0.14	<IQL	160	6.6
EPC 7-4	2.015	490	2.2	<IQL	330	0.50
EPC 7-6	3.015	190	0.86	0.46	160	2.1
EPC 7-8	4.015	110	0.67	0.63	110	4.0
EPC 7-9	5.015	100	0.47	1.2	78	7.4
EPC 7-11	6.015	70	0.41	1.1	59	10
EPC 7-12	7.015	43	0.19	<IQL	45	8.3
EPC 7-14	7.905	29	0.12	<IQL	30	4.9
EPC 7-15	9.015	33	0.13	<IQL	28	4.4
EPC 7-16	10.675	18	<IQL	<IQL	28	4.6
EPC 7-17	11.415	5.4	<IQL	<IQL	13	2.6
EPC 7-18	12.655	4.0	<IQL	<IQL	12	2.9
EPC 7-19	14.065	4.6	<IQL	<IQL	16	4.3
EPC 7-21	15.515	5.1	<IQL	<IQL	25	6.2
EPC 7-22	16.015	5.5	<IQL	<IQL	10	4.0
EPC 7-23	16.745	12	<IQL	<IQL	19	7.1

Table A- 4. Depth-weighted mass averages (mg kg^{-1}) for vadose zone anion concentrations.

Core	Total Depth (m)	Chloride (mg kg^{-1})	Bromide (mg kg^{-1})	Nitrate-N (mg kg^{-1})	Sulfate (mg kg^{-1})	Fluoride (mg kg^{-1})
EPC 1	5.1	4.5	0.33	0.017	28	1.2
EPC 2	5.2	4.4	0.33	0	30	1.7
EPC 5	11.7	6.6	0	0.12	24	3.3
EPC 7	16.7	69	0.31	0.20	64	4.8

Table A- 5. Daily rain and corresponding day in Hydrus 1D model simulation.

Date	Rain (mm)	Model Day	Date	Rain (mm)	Model Day	Date	Rain (mm)	Model Day	Date	Rain (mm)	Model Day
12/27/2016	0	1	2/7/2017	0	43	3/21/2017	0	85	5/2/2017	0	127
12/28/2016	0	2	2/8/2017	0	44	3/22/2017	0	86	5/3/2017	4.064	128
12/29/2016	0	3	2/9/2017	0	45	3/23/2017	0	87	5/4/2017	0	129
12/30/2016	0	4	2/10/2017	0	46	3/24/2017	12.45	88	5/5/2017	0	130
12/31/2016	0	5	2/11/2017	0	47	3/25/2017	0.254	89	5/6/2017	0	131
1/1/2017	0	6	2/12/2017	0	48	3/26/2017	0	90	5/7/2017	0	132
1/2/2017	0	7	2/13/2017	0	49	3/27/2017	0.508	91	5/8/2017	0	133
1/3/2017	0	8	2/14/2017	2.54	50	3/28/2017	0	92	5/9/2017	0	134
1/4/2017	0	9	2/15/2017	0	51	3/29/2017	35.81	93	5/10/2017	0	135
1/5/2017	0	10	2/16/2017	0	52	3/30/2017	18.03	94	5/11/2017	22.1	136
1/6/2017	0	11	2/17/2017	0	53	3/31/2017	0	95	5/12/2017	3.302	137
1/7/2017	0	12	2/18/2017	0	54	4/1/2017	0	96	5/13/2017	0	138
1/8/2017	0	13	2/19/2017	0	55	4/2/2017	12.95	97	5/14/2017	0	139
1/9/2017	0	14	2/20/2017	0	56	4/3/2017	0	98	5/15/2017	0	140
1/10/2017	0	15	2/21/2017	0	57	4/4/2017	0	99	5/16/2017	0	141
1/11/2017	0	16	2/22/2017	0	58	4/5/2017	11.43	100	5/17/2017	0.254	142
1/12/2017	0	17	2/23/2017	0	59	4/6/2017	0	101	5/18/2017	0	143
1/13/2017	0	18	2/24/2017	0	60	4/7/2017	0	102	5/19/2017	0	144
1/14/2017	0	19	2/25/2017	0	61	4/8/2017	0	103	5/20/2017	2.286	145
1/15/2017	0.762	20	2/26/2017	0	62	4/9/2017	0	104	5/21/2017	0	146
1/16/2017	2.286	21	2/27/2017	0	63	4/10/2017	0	105	5/22/2017	0	147
1/17/2017	11.18	22	2/28/2017	0	64	4/11/2017	0	106	5/23/2017	0.762	148
1/18/2017	2.286	23	3/1/2017	0	65	4/12/2017	0	107	5/24/2017	0	149
1/19/2017	0	24	3/2/2017	0	66	4/13/2017	79.25	108	5/25/2017	0	150
1/20/2017	0	25	3/3/2017	0	67	4/14/2017	0	109	5/26/2017	0	151
1/21/2017	0	26	3/4/2017	0	68	4/15/2017	0	110	5/27/2017	0	152
1/22/2017	0	27	3/5/2017	0	69	4/16/2017	0	111	5/28/2017	0.254	153
1/23/2017	0	28	3/6/2017	0	70	4/17/2017	0	112	5/29/2017	0	154
1/24/2017	0	29	3/7/2017	0	71	4/18/2017	0	113	5/30/2017	0	155
1/25/2017	0	30	3/8/2017	0	72	4/19/2017	0	114	5/31/2017	0	156
1/26/2017	0	31	3/9/2017	0	73	4/20/2017	0	115	6/1/2017	0	157
1/27/2017	0	32	3/10/2017	0	74	4/21/2017	0	116	6/2/2017	1.524	158
1/28/2017	0	33	3/11/2017	0	75	4/22/2017	5.588	117	6/3/2017	0	159
1/29/2017	0	34	3/12/2017	0	76	4/23/2017	0	118	6/4/2017	0	160
1/30/2017	0	35	3/13/2017	0	77	4/24/2017	0	119	6/5/2017	0	161
1/31/2017	0	36	3/14/2017	0	78	4/25/2017	0	120	6/6/2017	0	162
2/1/2017	0	37	3/15/2017	0	79	4/26/2017	0	121	6/7/2017	1.016	163
2/2/2017	0	38	3/16/2017	0	80	4/27/2017	0	122	6/8/2017	0	164
2/3/2017	0	39	3/17/2017	0	81	4/28/2017	6.604	123	6/9/2017	10.16	165
2/4/2017	0	40	3/18/2017	0	82	4/29/2017	4.318	124	6/10/2017	0	166
2/5/2017	0	41	3/19/2017	0	83	4/30/2017	20.32	125	6/11/2017	0	167
2/6/2017	0	42	3/20/2017	0	84	5/1/2017	10.92	126	6/12/2017	0	168
									6/13/2017	0	169

Table A- 6. Ion chromatograph instrument quantification limit (IQL) and R^2 value from linear regression. Values are based on two high and two low standards for each run. Detector response (area under the curve, µS*min) is plotted against the calculated standard quantities (mg L^{-1}) for the calculation of root mean square error (Corley, 2003).

Value	Fluoride	Chloride	Bromide	Nitrate-N	Phosphate-P	Sulfate
----------Run 1----------						
IQL	0.12	0.10	0.20	0.05	0.13	1.16
R^2	0.92	1.00	0.85	1.00	0.99	1.00
----------Run 2 ----------						
IQL	0.26	0.48	0.03	0.39	0.12	3.31
R^2	0.91	1.00	0.97	0.99	1.00	1.00
----------Average of Runs 1 and 2----------						
IQL	0.2	0.3	0.1	0.2	0.1	2.2
R^2	0.91	1.00	0.91	1.00	1.00	1.00

Table A- 7. Results for the four Infiltrometer measurements collected in August, 2017.

Test Name	Location	K_{sat} (cm sec^{-1})	K_{sat} (mm yr^{-1})	K_{sat} Error (cm sec^{-1})
Inf 1	Playa	7.84E-04	247,000	1.50E-04
Inf 2	Playa	1.62E-04	51,100	1.86E-05
Inf 3	Interplaya	2.33E-04	73,500	2.57E-04
Inf 4	Interplaya	7.21E-04	227,00	6.78E-05

Table A- 8. Fluid fluxes calculated from the date and time that each sensor reached field capacity (-33 kPa).

Sensor Depth (cm)	Date Field Capacity was Reached at Sensor	Time Elapsed Between Reaching Field Capacity (days)	Fluid Flux (mm yr^{-1})
12	3/29/17 11:30 AM	NA	NA
47	4/12/17 10:30 PM	14.46	8,800
96	4/13/17 9:20 AM	0.45	400,000
152	4/14/17 3:20 AM	0.75	270,000

Table A- 9. Maximum Fluid Flux calculated by the Hydrus 1D model at each of the four nodes.

Node (cm)	Max Flux (mm yr^{-1})
Surface	28,900
39	9,600
160	470
510	2.9E-06
1150	2.9E-06

Supplementary Figures Appendix 2

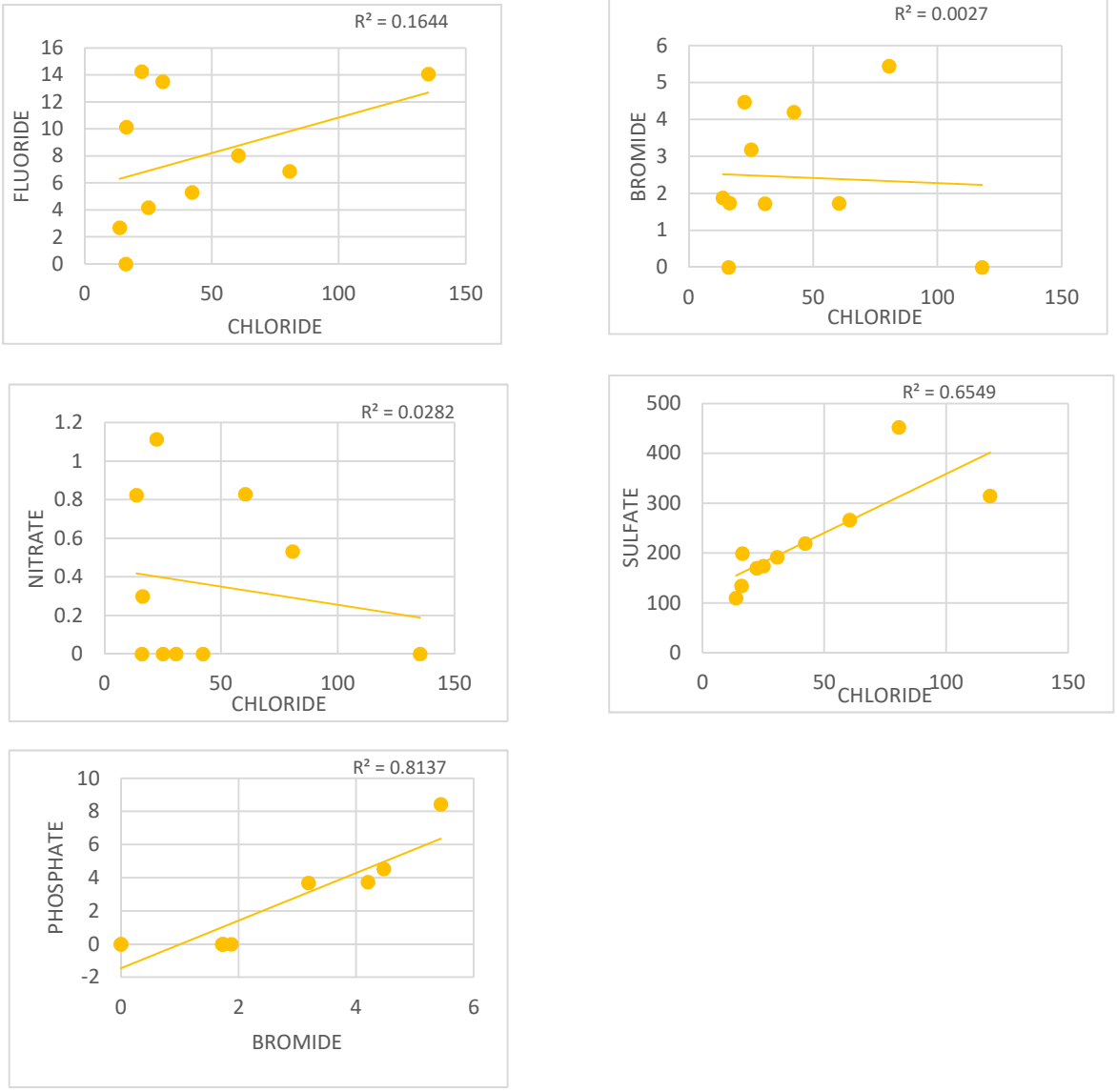

Figure A- 1. EPC 1 linear regression for vadose zone anion concentrations (mg L^{-1}). The best-fit line is shown and the calculated correlation coefficient (R^2).

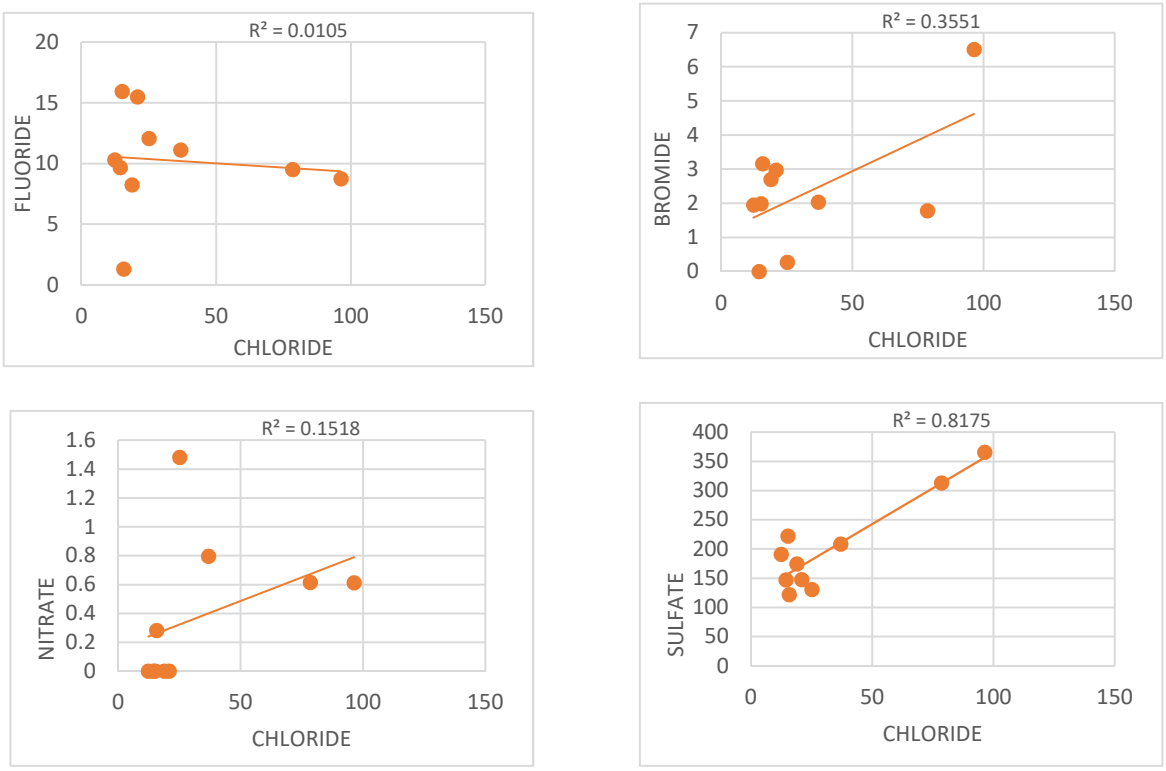

Figure A- 2. EPC 2 linear regression for vadose zone anion concentrations (mg L^{-1}). The best-fit line is shown and the calculated correlation coefficient (R^2).

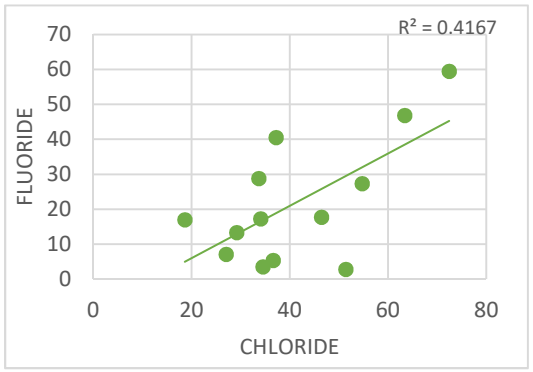

Bromide is <IQL in this profile

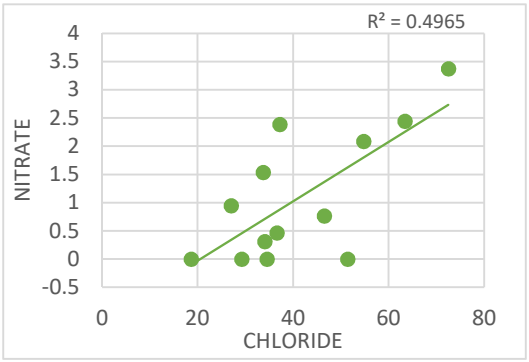

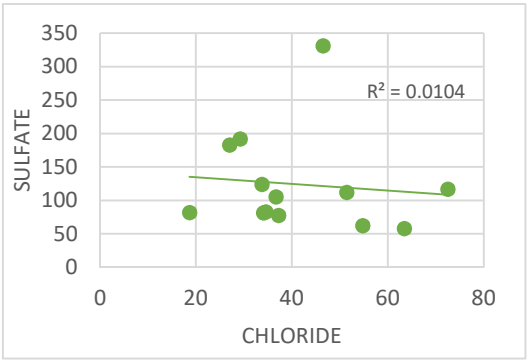

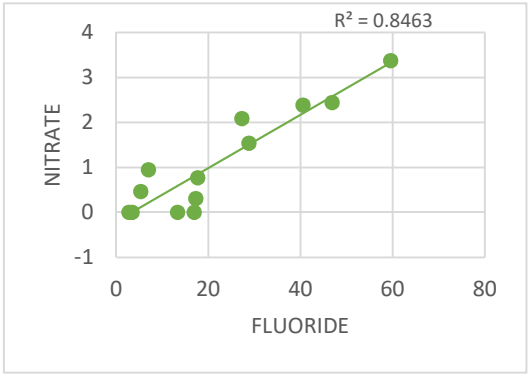

Figure A- 3. EPC 5 linear regression for vadose zone anion concentrations (mg L^{-1}). The best-fit line is shown and the calculated correlation coefficient (R^2). Bromide levels are below the instrument quantification limit shown in Table A- 6.

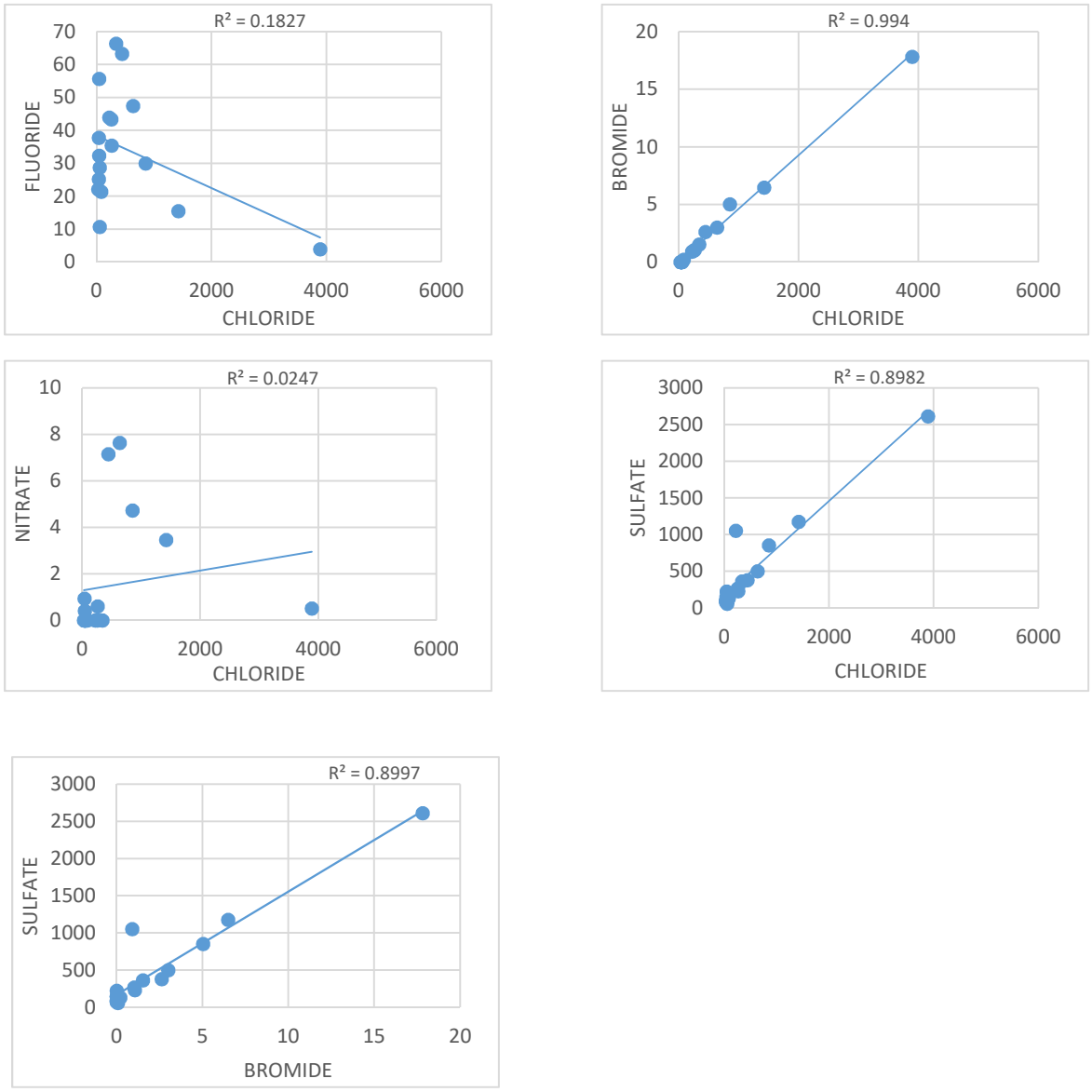

Figure A- 4. EPC 7 linear regression for vadose zone anion concentrations (mg L^{-1}). The best-fit line is shown and the calculated correlation coefficient (R^2).

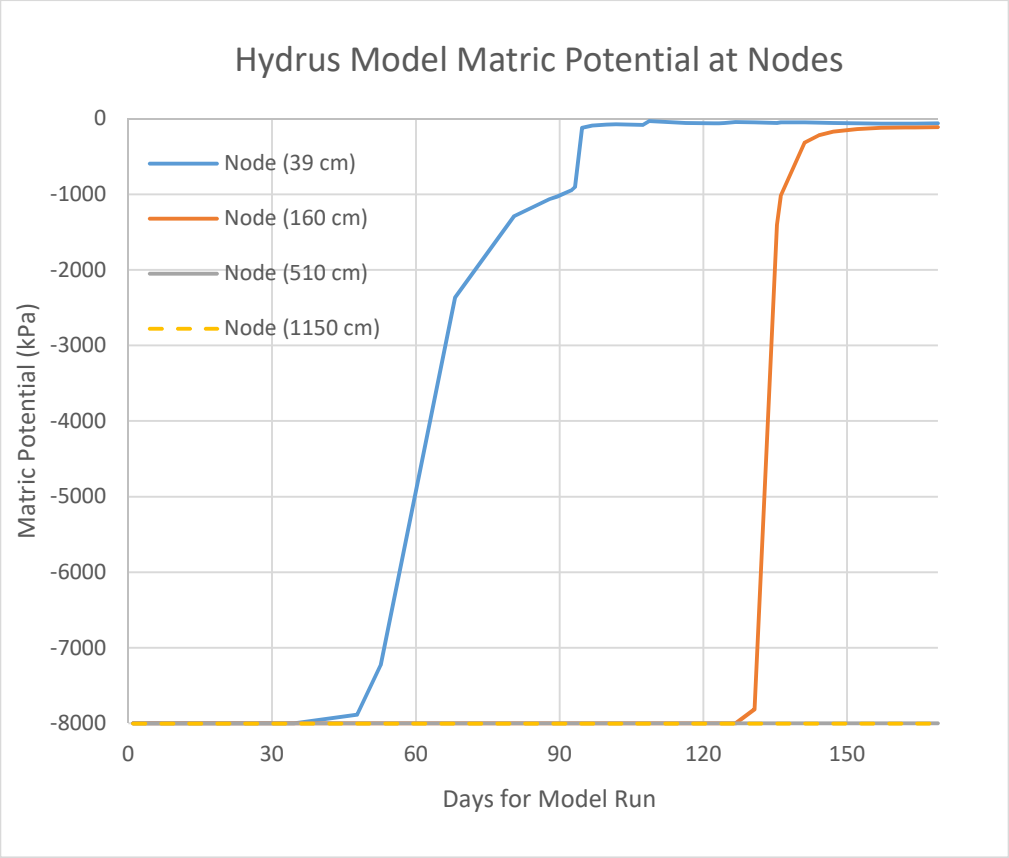

Figure A- 5. Simulated matric potential at nodes from Hydrus 1D model.

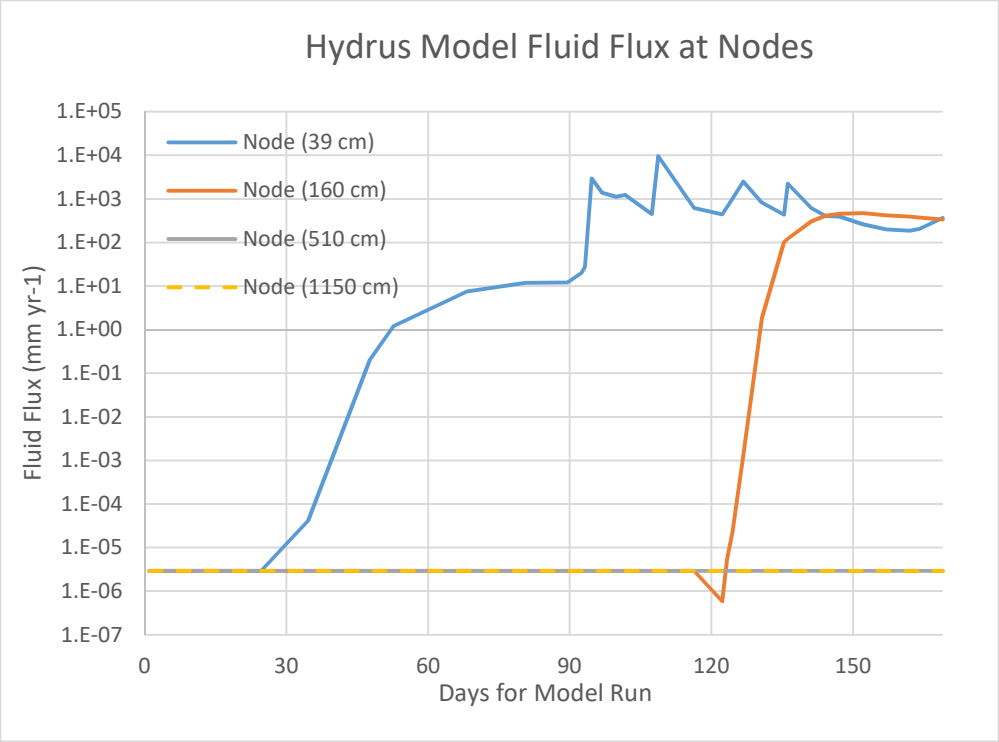

Figure A- 6. Simulated fluid flux at nodes from Hydrus 1D model.

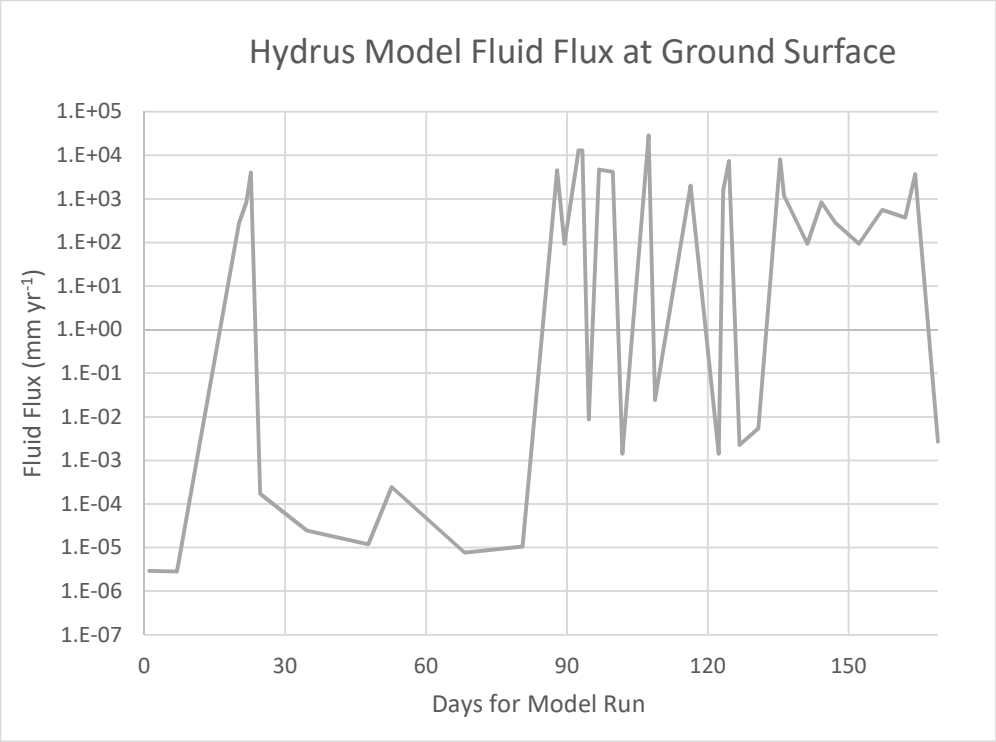

Figure A- 7. Simulated infiltration at the ground surface from the Hydrus 1D model.

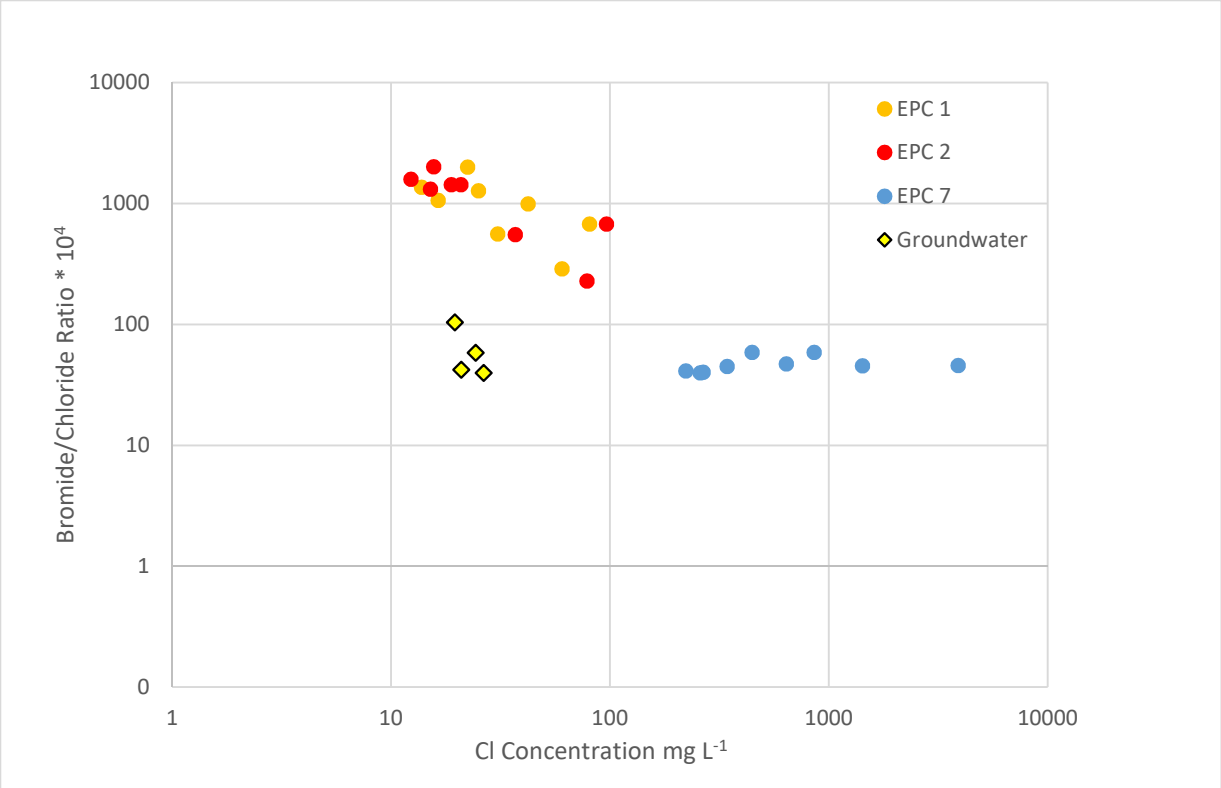

Figure A- 8. Bromide/chloride mass ratios (multiplied by 10^4) are plotted against chloride concentration.

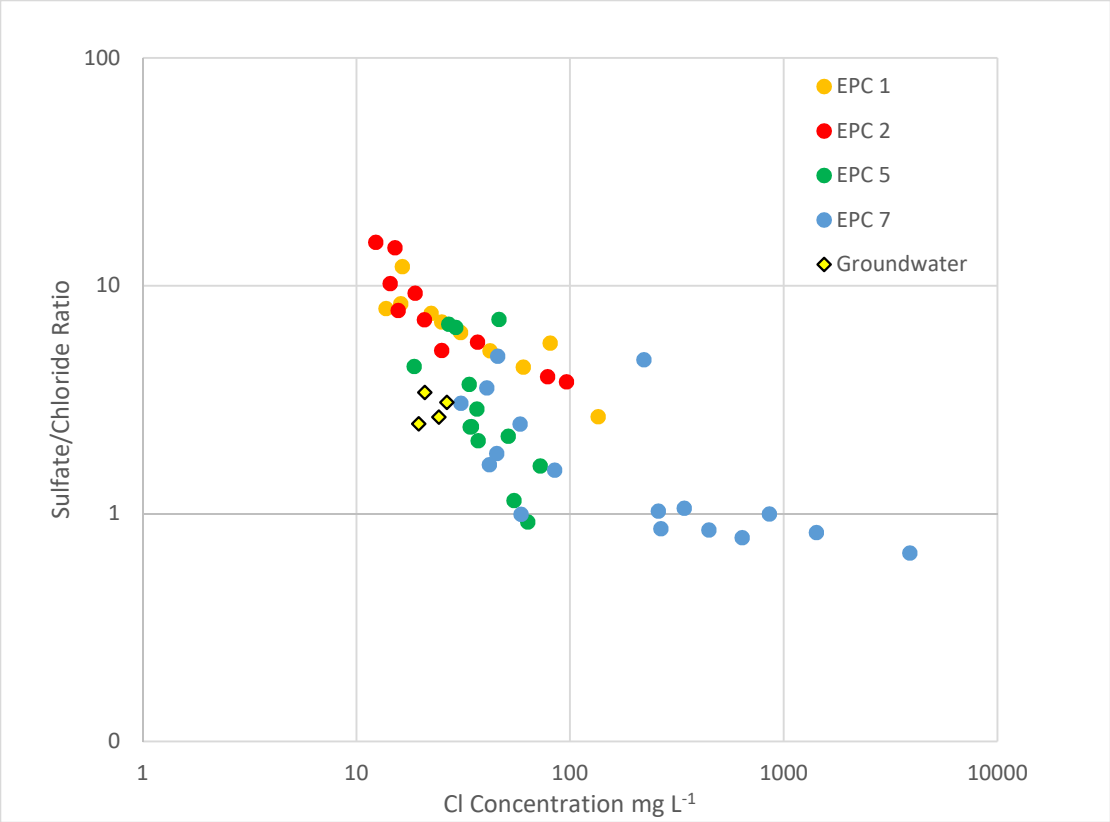

Figure A- 9. Sulfate/chloride mass ratios plotted against chloride concentration.

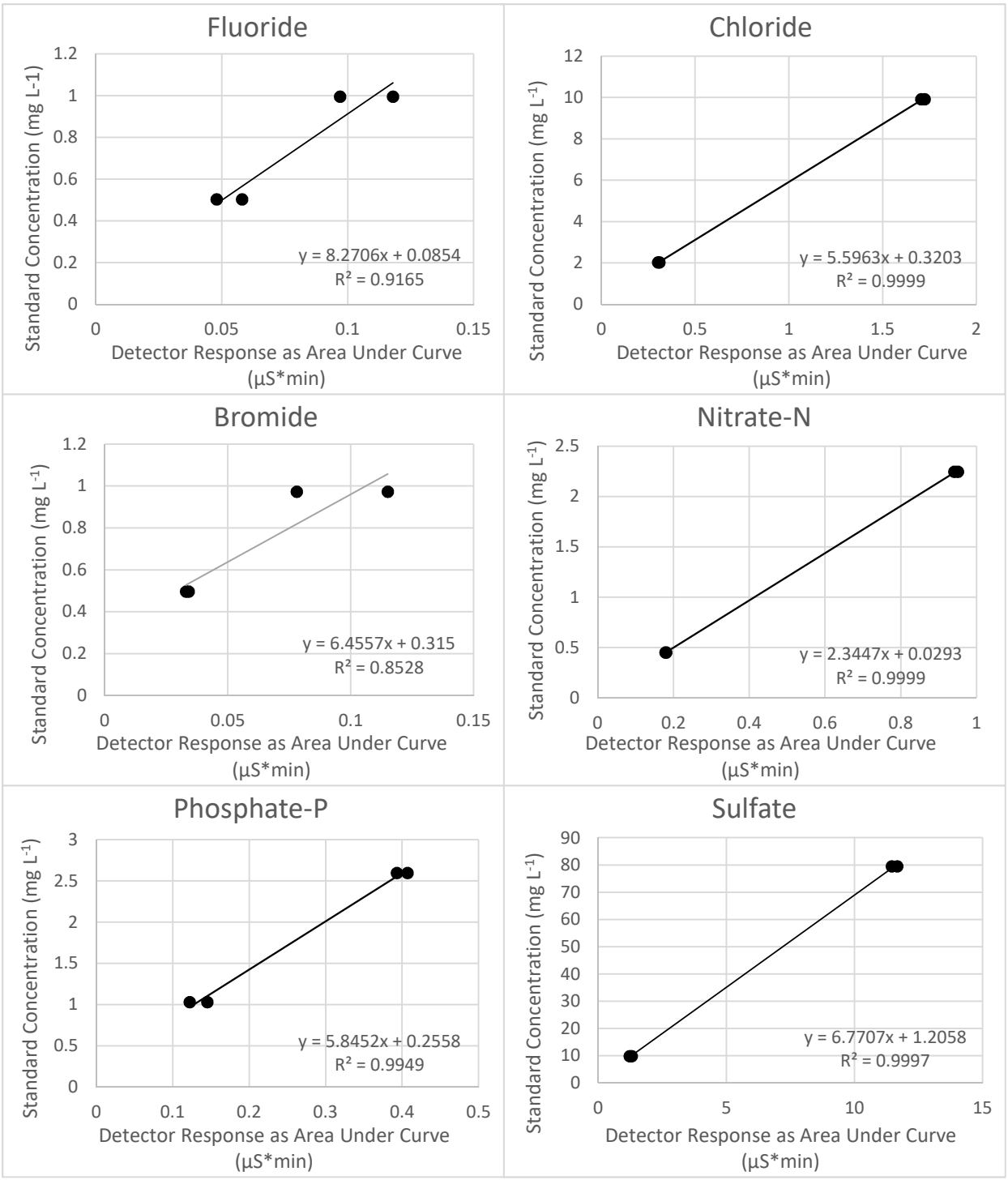

Figure A- 10. Ion chromatograph run 1 from July 2017. Two high and two low standards are plotted in each graph, detector response (as the area under the curve) is plotted against calculated standard concentration, and a best-fit line drawn for calculation of slope, y-intercept, and R^2. These values are then utilized in the root mean square error calculation for the instrument quantification limits shown in Table A- 6.

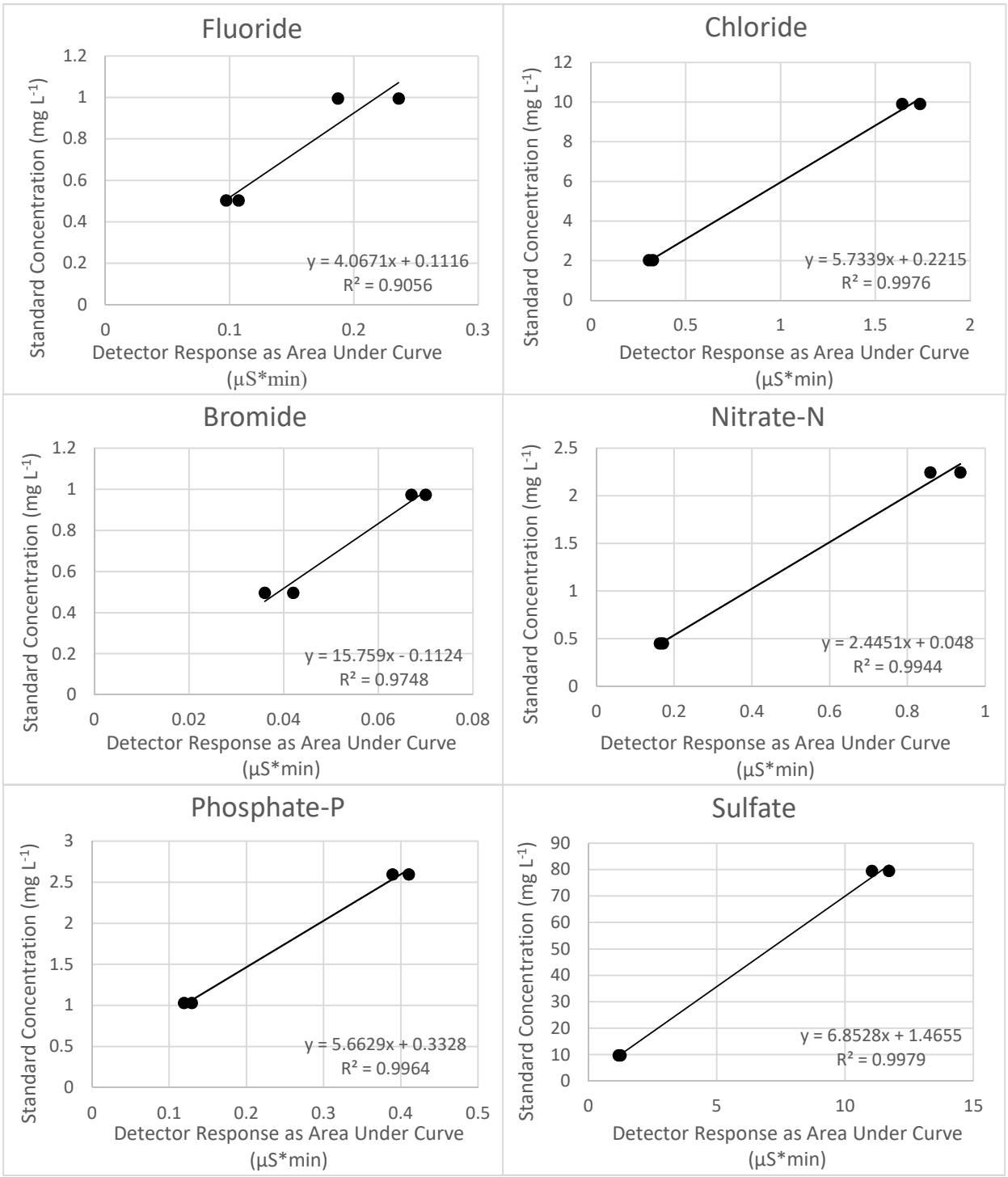

Figure A- 11. Ion chromatograph run 2 from October 2017. Two high and two low standards are plotted in each graph, detector response (as the area under the curve) is plotted against calculated standard concentration, and a best-fit line drawn for calculation of slope, y-intercept, and R^2. These values are then utilized in the root mean square error calculation for the instrument quantification limits shown in Table A- 6.

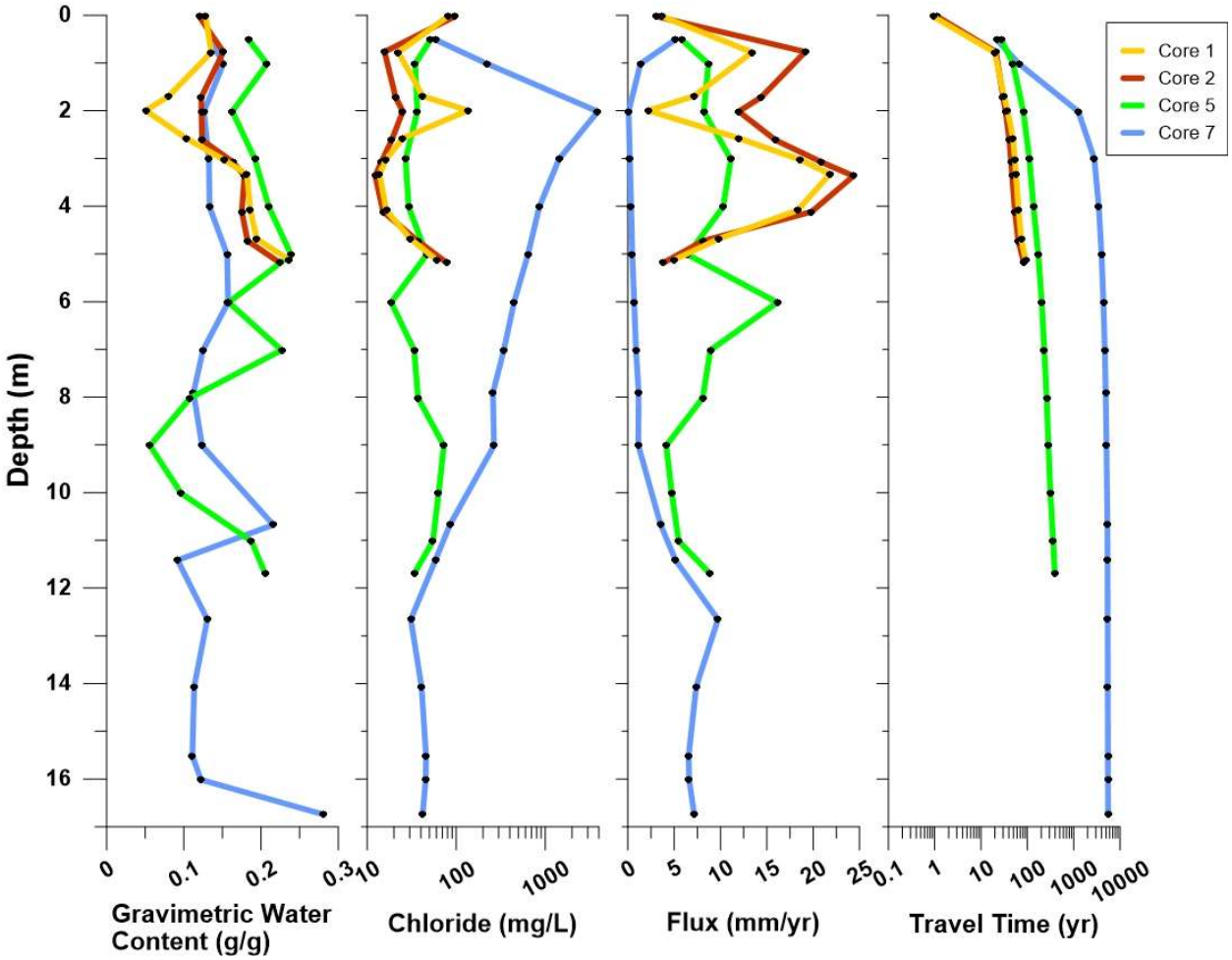

Figure A- 12. Depth profiles (in m below ground surface) for playa (EPC 1, 2, 5) and interplaya core (EPC 7) with gravimetric water content, chloride concentration in vadose zone pore water, fluid flux rate from Equation 4 the Chloride Mass Balance (CMB) method, and travel time to the water table from the CMB method.

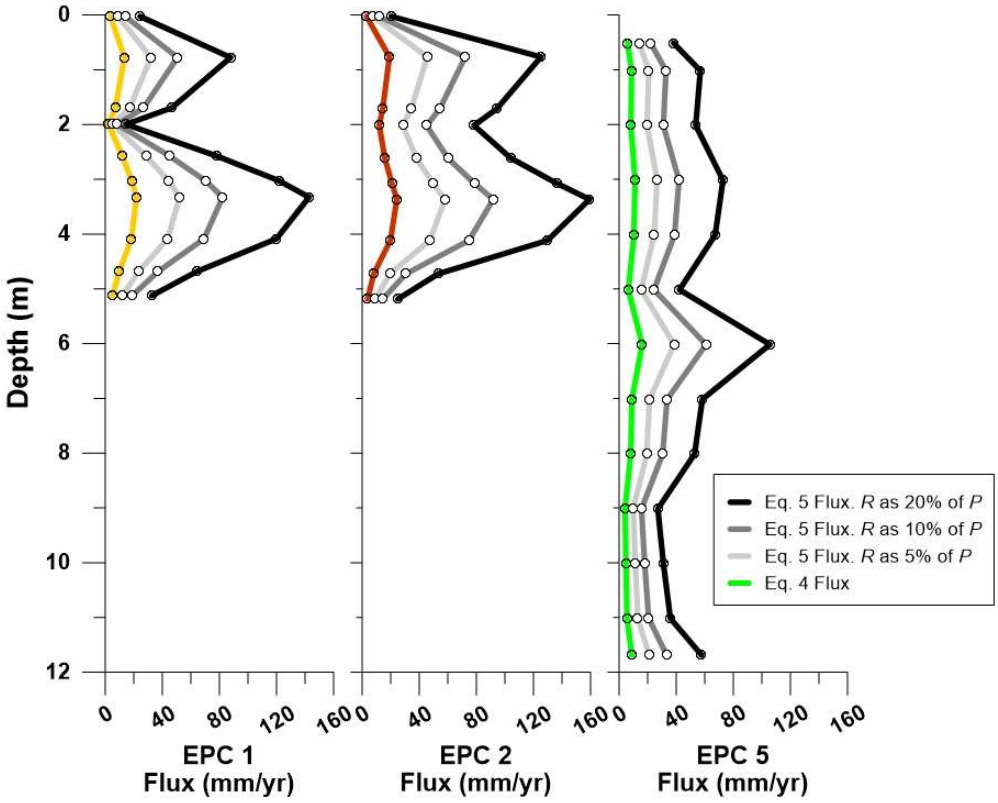

Figure A- 13. Variations in playa flux from 2016 (EPC 1 and 2) and 2017 (EPC 5) cores. Colored lines correspond to flux displayed in Figure A-12 and calculated from Equation 4. Remaining lines are calculated from Equation 5 with the run-off from surrounding basin as 5%, 10%, and 20% of annual precipitation.